
# Transmutation of Am in sodium fast reactors and accelerator driven systems

YOUPENG ZHANG

Doctoral Thesis, Stockholm, Sweden, 2012

**Abstract**

In this thesis, the feasibility to use sodium cooled fast reactors loaded with MOX, metallic and nitride fuels for efficient transmutation of americium is investigated by performing transient analysis for cases with different americium contents in fuels, using safety parameters obtained with the SERPENT Monte Carlo code. It was then demonstrated that there is no solid limit for the Am introduction into oxide, metallic and nitride fuels that were loaded into sodium fast reactors. Instead, higher Am contents could be permitted if specific levels of power penalty were accepted.

Transient analysis of a new Accelerator Driven System design with higher neutron source efficiency than the reference EFIT-400 design, was also performed. Based on simulation results, the suggested ADS design was proved to survive the full set of transients, preserving 130 K margin to cladding rupture during the most limiting transient.

After comparing Am transmutation performances in SFRs and the suggested ADS, it can be concluded that: 1. Nitride fuel could provide the highest Am transmutation efficiency, when loaded into SFRs; 2. One SFR loaded with nitride fuel is sufficient to transmute Am inventory produced by more than 15 commercial LWRs within the same time period, which is three times higher than the supporting ratio reported for the suggested ADS; 3. The total fraction of ADS power in the power park is half of cases for critical reactors.

# Acknowledgements

First of all, I want to express my sincerest appreciation to my supervisor, Prof. Janne Wallenius, who has supported me throughout my PhD studying and thesis writing with his patience and knowledge.

I also want to express my gratitude to Mikael, Milan and Andrei for being fantastic co-authors of some of my papers; Dr. Daniel Westlén and Dr. Marcus Eriksson who aroused my passion on reactor physics before I started my PhD career four years ago.

In my daily work I have been blessed with my friendly colleagues: Zhongwen as my officeate sharing wonderful talks and discussions on both physics and fun moments in life; Michael as an encyclopedia-type advisor for almost everything; Nils for precious comments on material science and also as the best ski instructor; Vasily for cooperation of the lab teaching and also instructive stories.

To Odd Runevall and Jan Dufek, thanks for your comments on my first journal paper, which is really an important step.

I want to thank the wonderful working circumstance created by Pär, Jitka, Pertti, Luca, Meg, Merja, Farnaz, Qi Chong and Xu Zhenxiang.

This research was financially supported by Svensk Kärnbränslehantering AB (SKB).

The Department of Physics has provided the support and equipment I have needed to accomplish my studies.

Finally, I want to show my thanks to my parents for encouraging on my PhD study and also my girlfriend for taking care of my life in Sweden.

# List of Papers

## Publications

1. Youpeng Zhang, Janne Wallenius and Andrei Fokau, *Transmutation of Americium in a Medium Size Sodium Cooled Fast Reactor Design*, Annals of Nuclear Energy, **37**(5): 629-638, 2010.

2. Youpeng Zhang, Andrei Fokau, Shinya Ishida and Janne Wallenius, *Physics and safety studies of a compact ADS design loaded with nitride fuel*, Annals of Nuclear Energy, **38**(11): 2350-2355, 2011.

3. Youpeng Zhang, Janne Wallenius, *Upper limits to americium concentration in large sized sodium-cooled fast reactors loaded with metallic fuel*, Nuclear Science and Engineering, submitted, 2011.

4. Youpeng Zhang, Janne Wallenius, Mikael Jolkkonen, *Transmutation of americium in a large sized sodium-cooled fast reactor loaded with nitride fuel*, Annals of Nuclear Energy, submitted, 2011.

5. Andrei Fokau, Youpeng Zhang, Shinya Ishida, Janne Wallenius, *A source efficient ADS for minor actinides burning*, Annals of Nuclear Energy, **37**(4):540-545, 2010.

## Author's Contribution

In the first four papers listed above, reactor performance parameters and reactivity coefficients were calculated with the SERPENT Monte Carlo code by the author. Besides, transient analysis were performed with the SAS4A/SASSYS code by the author for all five papers.

## Papers Not Included

1. Milan Tesinsky, Youpeng Zhang, Janne Wallenius, *The impact of Americium on the ULOF and UTOP transients of the European lead-cooled system ELSY*, Annals of Nuclear Energy, submitted, 2011.

2. W. Maschek, C. Artioli, X. Chen, F. Delage, A. Fernandez-Carretero, M. Flad, A. Fokau, F. Gabrielli, G. Glinatsis, P. Liu, L. Mansani, C. Matzerath Boccaccini, C. Petrovich, A. Rineiski, M. Sarotto, M. Schikorr, V. Sobolev, S. Wang, Y. Zhang, Design, *Safety and Fuel Developments for the EFIT Accelerator Driven System with CERCER and CERMET Cores*, Actinide and Fission Product Partitioning and Transmutation, 10th OECD/NEA Information Exchange Meeting, Mito, Japan, 2008.

3. Youpeng Zhang and Janne Wallenius, *Upper Limits to Americium Concentration in Medium Size Sodium Cooled Fast Reactors*, Global 2009, Paris, France, 2009.

# Nomenclature

| | |
|---|---|
| ADS | Accelerator Driven System |
| BOC | Beginning of Cycle |
| CW | Cold Worked, a work hardening process to enhance mechanical properties of metals |
| DHR | Decay Heat Removal |
| EBR-II SHRT | Shutdown Heat Removal Test on Experimental Breeder Reactor |
| EFIT | European Facility for Industrial Transmutation |
| EOC | End of Cycle |
| EOEC | End of Equilibrium Cycle |
| FBR | Fast Breeder Reactor, conversion ratio higher than 1.0 |
| FCCI | Fuel-Cladding Chemical Interaction |
| FCMI | Fuel-Cladding Mechanical Interaction |
| FIMA | Fission in Metal Atoms |
| FP | Fission Products |
| GEMs | Gas Expansion Modules |
| GeV | Giga electron Volts |
| GFR | Gas-cooled Fast Reactor |
| HLM | Heavy Liquid Metal |

| | |
|---|---|
| HLW | High Level Waste |
| HTR | High Temperature gas-cooled Reactor |
| IFR | Integral Fast Reactor |
| LBE | Lead-bismuth Eutectic |
| LFR | Liquid-metal-cooled Fast Reactor |
| LINAC | LINear ACcelerator |
| LLW | Low Level Waste |
| MA | Minor Actinides, i.e., Np, Am, Cm |
| MeV | Mega electron Volts |
| MLW | Medium Level Waste |
| MOX | Mixed OXide, a compound of $PuO_2$ and $UO_2$ |
| $MW_e$ | Megawatt electrical |
| $MW_{th}$ | Megawatt thermal |
| PDS-XADS | Preliminary Design Studies of an Experimental Accelerator Driven System |
| PLOHS | Protected Loss-of-Heat-Sink |
| RF | Radio Frequency |
| SFR | Sodium-cooled Fast Reactor |
| TREAT M-series | Transient REActor Test facility, series tests for Metallic fuel in Mark-III sodium loop |
| ULOF | Unprotected Loss-of-Flow |
| ULOOP | Unprotected Loss-of-offsite-Power |
| UTOP | Unprotected Transient-over-Power |
| UOX | Uranium OXide |
| XTADS | eXperimental facility demonstrating the technical feasibility of Transmutation in an Accelerator Driven System |

# Contents

# Chapter 1

# Introduction

## 1.1 Nuclear waste

Nuclear waste, containing radioactive materials, is a by-product discharged by nuclear power plants, nuclear research facilities or even medical devices. Among them, nuclear power plants are the major contributors in the nuclear waste stockpile.

Nuclear waste can be divided into three main groups based on their corresponding radioactivity as listed in Table 1.1. Since nuclear radiation has been proved to be hazardous to human being and also other living creatures in biosphere, nuclear waste should be carefully managed.

**Table 1.1.** Nuclear waste categories [1] [2]

| Type | Radioactivity (Bq/g) | Content |
|---|---|---|
| LLW | $\sim 5\times10^5$ | Stuff contaminated by radioactive materials |
| MLW | $5\times10^5$ $\sim5\times10^8$ | Irradiated structure material and milling waste |
| HLW | $5\times10^8$ $\sim$ | Irradiated or used nuclear fuel |

Low and intermediate level wastes (LILW) produced by nuclear power plants are mainly materials in nuclear power plants (e.g., water coolant, filter parts, inner structure) contaminated by radiotoxic nuclides generated from nuclear fission (e.g., I-129) or particle activation (e.g., Co-60 and Ni-63). Volume reduction of these low and intermediate level wastes into either liquid, gas or solid phases should be accomplished, aiming at a lower disposal cost [3]. Several methods and technologies have been proposed by different countries in order to achieve the volume reduction of LILW as listed in Table 1.2. It can be observed that all the volume reduction technologies for LILW inventory could provide a quite satisfying reduction factor [4].

**Table 1.2.** LILW phases and corresponding volume reduction treatments

| Phase | Treatment | Reduction Factor,vol.% |
|---|---|---|
| Liquid+soluble particles | Evaporation | $\sim 100$ |
| | Chemical precipitation | – |
| Liquid+insoluble particles | Filter, centrifugal, hydrocyclones | – |
| Gas | HEPA filters, Charcoal filter | $\sim$90 |
| Solid | Incineration | 50$\sim$80 |

However, since the radioactivity of HLW is orders of magnitude higher than LILW [5] and the major part of HLW is not combustible, volume reduction of the solid HLW by incineration treatment is neither necessary nor possible. Instead, in order to eliminate the radiotoxicity of HLW, either the inventory of radioactive nuclides or the radioactivities of nuclides in HLW should be reduced.

Radioactive nuclides in HLW mainly consists of radioactive fission products and transuranic isotopes, e.g. $^{239}$Pu, $^{240}$Pu, $^{241}$Am, $^{243}$Am [6].

Fission products can be divided into long-lived and short-lived types based on their decay half-life times. The short-lived fission products, e.g. $^{137}$Cs, $^{90}$Sr, are major decay heat emitter during the short-term storage or cooling process of spent fuel, which is a tens of years or hundreds of years period at most. Since the integrity and safeguard condition of nuclear waste can be insured for these timescales, the short lived fission products are not issues in present study. Comparing to other long-lived fission products (LLFP), e.g., $^{93}$Zr and $^{135}$Cs, $^{99}$Tc and $^{129}$I are more hazardous not only because of their higher radiotoxicities but also because of their higher chemical mobility [7][8], which is a key issue for long-term storage of radioactive nuclear wastes. Still, the accumulated dose from fission products over million years' timescale was calculated to be negligible [9] [10].

However, comparing to that released from radioactive actinides, especially transuranic nuclides, the decay energy released from LLFP nuclides is still negligible [11].

As can be noticed from Table 1.3, plutonium isotopes dominate the transuranic inventory ($\approx$90 wt.%) discharged from light water reactors, leading to the major contribution to the radioactivity of spent fuel as can be noticed from Fig. 1.1. Some Pu isotopes, such as $^{238}$Pu, having short $\alpha$-decay half-life times (e.g., $T_{1/2,\alpha}$ of $^{238}$Pu $\approx$ 86 years), are intensive decay heat emittors, which leads to difficulties for spent fuel handling and also necessities for cooling process before fuel reprocessing. Americium and curium isotopes bred from neutron capture starting from uranium isotopes will be even more troublesome for the spent fuel handling due to neutron source generated by spontaneous fissions and ($\alpha$,n) reactions, in addition to high levels of decay heat [14].

**Table 1.3.** Decay characteristics of major transuranic actinides in spent fuel from LWRs [12]

| Isotope | Mass fraction 50 MWd/kgHM | Half-life Total, year | Half-life SF, year |
|---|---|---|---|
| Np-237 | 5.33 | $2.14\times10^{6}$ | – |
| Pu-238 | 3.11 | 86.41 | $4.77\times10^{10}$ |
| Pu-239 | 46.15 | $2.41\times10^{4}$ | $8.00\times10^{15}$ |
| Pu-240 | 21.19 | $6.56\times10^{3}$ | $1.16\times10^{11}$ |
| Pu-241 | 11.48 | 14.40 | $6.00\times10^{16}$ |
| Pu-242 | 7.03 | $3.75\times10^{5}$ | $6.77\times10^{10}$ |
| Am-241 | 2.81 | $4.33\times10^{2}$ | $1.00\times10^{14}$ |
| Am-243 | 2.07 | $7.37\times10^{3}$ | $2.00\times10^{14}$ |
| Cm-244 | 0.74 | 18.10 | $1.32\times10^{7}$ |
| Cm-245 | 0.07 | $8.48\times10^{3}$ | $1.40\times10^{12}$ |

## 1.2 Transmutation

The terminology "transmutation" was defined as a physical process of changing one element to another. In nuclear fuel treatments, "transmutation" stands for the process of conversing long-lived nuclides with high radiotoxicities to short-lived ones with lower radiotoxicities. These targets could be achieved by fissioning long-lived transuranic nuclides or by converting LLFP nuclides (e.g., $^{99}$Tc and $^{129}$I) into short-lived ones through neutron absorption.

In order to transmute LLFP, high thermal and/or epi-thermal neutron flux is needed since capture cross sections of major nuclides in LLFP are higher in these energy spectrum as shown in Fig. 1.3. Possibilities of transmuting LLFP in several devices, being able to provide the required neutron flux, have been investigated [9].

- In HFR in Petten, transmutation rates of LLFP up to 50% within 3 years has been reported. However, due to the impact from FP introduction on reactor parameters, the amount of FP that could be loaded into high flux reactors is limited. Hence, only a small transmutation efficiency of LLFP can be expected from high flux reactors.

- In commercial light water reactors, due to an order of magnitude lower neutron flux, the transmutation rate of LLFP that can be achieved is much lower than in high flux reactors. This will lead to a heavy burden on fuel reprocessing.

- Heavy water moderated reactors, e.g., CANDU, might be a good choice because of the high thermal neutron flux they could provided and also flexible loading plans they permitted. However, feasibility of this proposal still needs more validations [9].

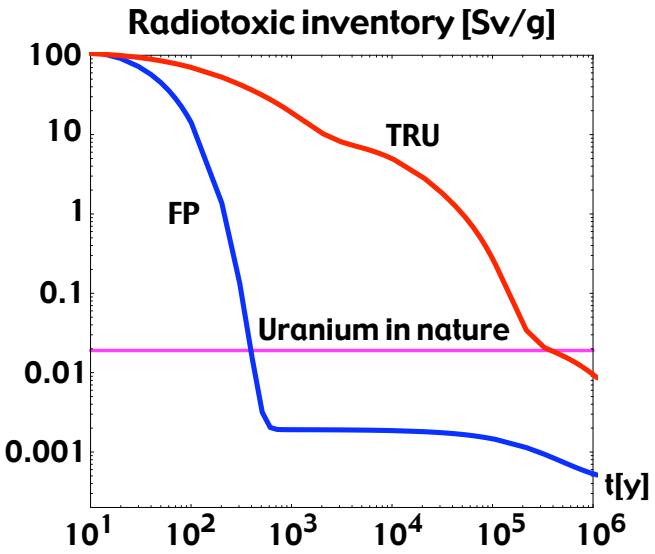


**Figure 1.1.** Radiotoxicity evolution with time [13]

- Accelerator driven system, permitting bigger amount of FP to be loaded thanks to the introduction of strong accelerator driven external neutron source, is proposed to be another choice, but it is not acceptable on the economic point of view.

Since the radiotoxicity of fission products will be lower than that of natural uranium after approximately 300 years as shown in Fig. 1.1, LLFP in spent fuel will not be an issue after several hundred years storage, the safety and integrity of which can be well insured by existing technologies and strategies. However, if human intrusion (hard to be prevented in a long time scale as discussed above) happened, hazard from long-lived actinides may last for more than thousands of years or even tens of thousands of years, which is even longer than the history of human civilization. The reliability of current safe-guarding strategies for nuclear waste disposal in this long time scale is hard to be confirmed. Thus, burning the long-lived actinides becomes the major motivation for spent fuel transmutation.

If transuranic inventory, including Am and Cm, discharged from LWRs was multi-recycled in advanced PWR, the long-term radiotoxic inventory could be reduced by a factor of 200 [15]. However, since fission probabilities of transuranic actinides containing even number of neutrons, e.g., $^{241}$Am and $^{243}$Am, are negligibly small in a thermal neutron spectrum and will increase with incident neutron energy, fast neutron facilities are expected to be more efficient for transmutation of these transuranic nuclides, comparing to thermal neutron reactors. Besides, due

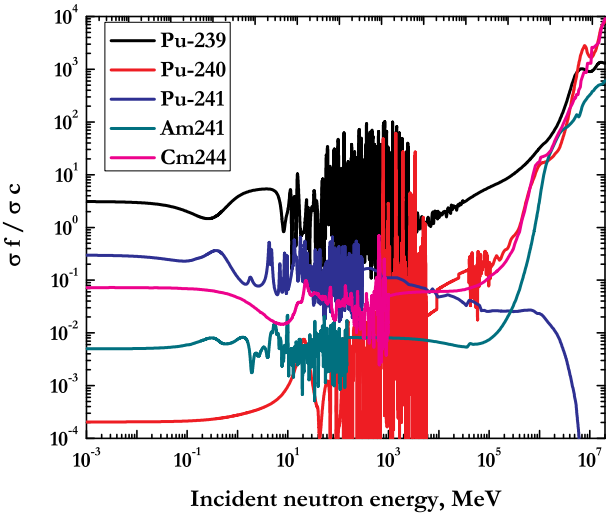


**Figure 1.2.** Fission-to-capture ratios of transuranic nuclides

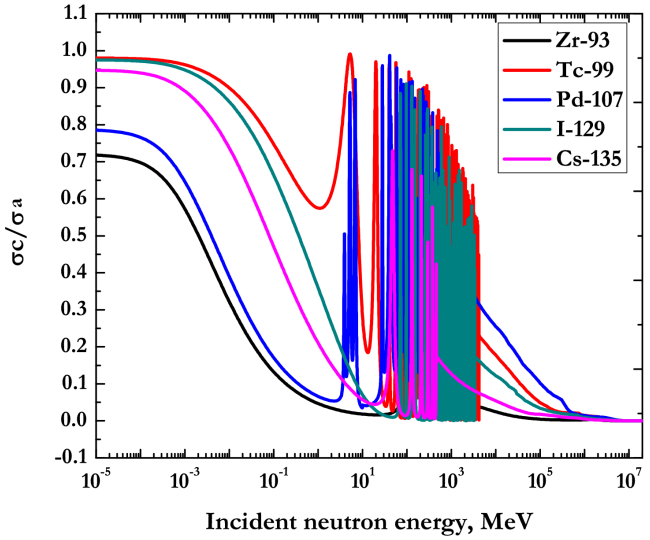


**Figure 1.3.** Capture-to-absorption ratios of LLFP

to high probabilities of neutron capture, actinides with even neutron number will more likely be bred into heavier nuclides (e.g. $^{252}$Cf) instead of being fissioned into relatively short-lived fission products. This may lead to the accumulation of $^{252}$Cf, being a strong neutron source, and then difficulties for spent fuel handling after several rounds of recycling processes.

# Chapter 2

# Fast-neutron facilities

As discussed above, transmutation of transuranic nuclides, especially minor actinides, is more efficient in fast neutron spectrum. Hence, in this chapter, different types of fast reactors and Accelerator Driven System (ADS) technology are briefly introduced.

## 2.1 Fast neutron reactors

Fast neutron reactors, or fast reactors in short, are reactors using fast neutrons to sustain chain reactions. As can be observed in Fig. 2.1, more fission neutrons could be released per neutron absorption in fuel in a fast neutron spectrum comparing to cases in a thermal neutron spectrum [16] , besides the ones used to maintain the chain reaction, there may be more neutrons available to breed fertile $^{238}$U into fissile $^{239}$Pu, through neutron capture followed by $\beta$ decay reactions as shown in Eq. 2.1. Theoretically, the fission neutron yield per fissile nuclide absorption higher than 2.0, including one fission neutron needed to sustain chain reactions and the other fission neutron used to breed new fissile nuclide, is adequate to provide a conversion ratio equal to unity. However, there are still possibilities for neutrons to leak out from core active zone or to be captured by fission products, coolant, inner structure material, control rods in reactor core. Therefore, the U-Pu cycle in a well thermalized spectrum is hardly feasible for achieving a conversion ratio $\geq$1.0.

$$\mathrm{n} + ^{238}\mathrm{U} \Rightarrow ^{239}\mathrm{U} + \gamma \Rightarrow ^{239}\mathrm{Np} + \beta^{-} \Rightarrow ^{239}\mathrm{Pu} + \beta^{-} \tag{2.1}$$

Fast neutron reactors were initially promoted to make a better usage of U resources by breeding fissile $^{239}$Pu nuclides from fertile $^{238}$U nuclides. Some countries even raised extensive research on fast breeder reactors aiming at producing more fissile materials, concerning the fissile material shortage. However, by 1970s, geological exploration showed that the uranium shortage will not become a problem in the near future, limiting the necessity for commissioning more fast reactors in the following years. Recently, thanks to the higher transmutation capability of long-lived transuranic isotopes comparing to light water reactors, fast reactors were

promoted again, aiming at reducing the HLW stockpile and shorten the time needed for geological storage.

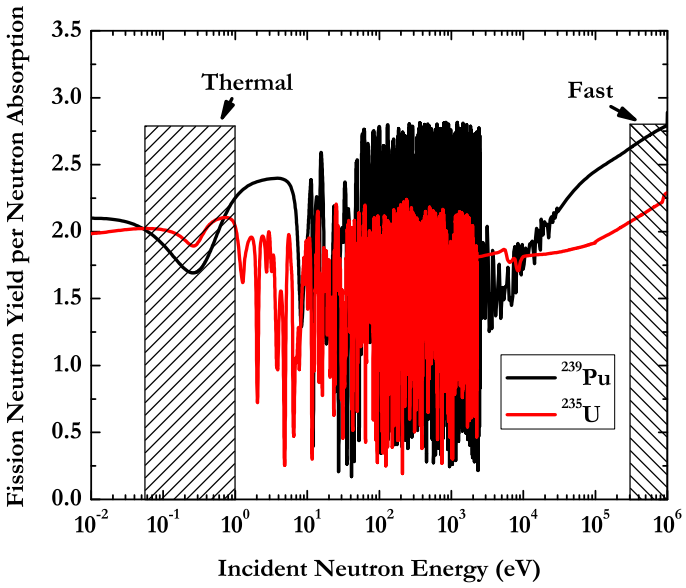


**Figure 2.1.** Fission neutron yields per neutron absorption in fuel

Besides, as can be noticed from Fig. 2.2, transuranic nuclides with even neutron numbers, e.g., $^{238}$Pu, $^{240}$Pu, $^{242}$Pu, $^{241}$Am, $^{243}$Am, $^{244}$Cm and $^{246}$Cm, have much higher probabilities to undergo fission in a fast neutron spectrum than in a thermal neutron spectrum, leading to a much lower accumulation of highly radioactive $^{252}$Cf. Therefore, when recycling transuranic isotopes in a fast neutron spectrum, the neutron activity of transuranic inventory was reported to drop by two orders of magnitude comparing to recycling transuranic inventory in a thermal neutron spectrum [17].

In order to get a fast neutron spectrum, coolant moderation power and absorption should be minimized. Water and organic materials, are then excluded due to large scattering cross sections of C and H nuclides and also large energy losses for neutrons during collisions. Thus, liquid Na, liquid Pb and chemically inert gases (e.g. He) are recommended for Gen-IV reactors as shown in Fig. 2.3.

### 2.1.1 Sodium-cooled fast reactor (SFR)

As the most mature fast reactor technology, not only prototype but also half commercial SFR units have been commissioned. Actually, except for the first few experimental reactors operated in 1940s and 1950s, e.g. CLEMENTINE (US), BR-I

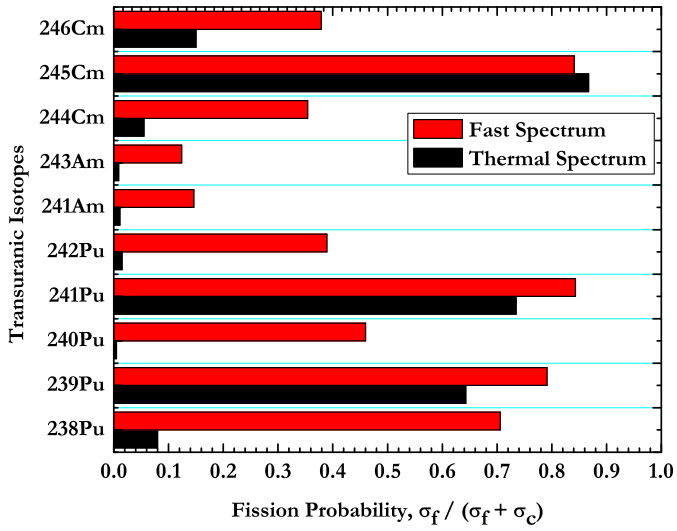


**Figure 2.2.** Spectrum-averaged fission probabilities of transuranic isotopes in a sodium cooled core and a PWR, loaded with oxide fuel

(USSR) and EBR-I (US), liquid Na was implemented as primary coolant for all fast neutron reactors, especially fast breeder reactors, thanks to: first, the maximum allowable Na velocity through pin bundles, having been reported to be 8.0 m/s [19][20], is not determined by concerns for corrosion on stainless steel surface but by concerns for the flow-induced vibration, which is highly sensitive to cylindrical structures. Since the maximum allowable velocity of liquid Na flow passing through fuel bundles is quite high, as well as the heat capacity, the minimum allowed coolant flow area for liquid Na could be quite small, preserving a specific temperature increase from core inlet to outlet ($\Delta$T) and heat removal rate calculated by

$$\begin{aligned} Q &= \dot{m} \times C_{\mathrm{p}} \times \Delta T_{\mathrm{coolant}} \\ &= \rho \times v_{\mathrm{coolant}} \times A_{\mathrm{coolant}} \times C_{\mathrm{p}} \times \Delta T_{\mathrm{coolant}} \end{aligned} \tag{2.2}$$

in which Q, $\dot{m}$, $\mathrm{C_p}$, $\Delta\ \mathrm{T_{coolant}}$, $\rho$, $\mathrm{v_{coolant}}$ and $\mathrm{A_{coolant}}$ stand for heat removal rate (W), flowrate (kg/s), heat capacity (J/kg/K), temperature increase (K), coolant density ($\mathrm{kg/m^3}$), coolant velocity (m/s) and flow channel area ($\mathrm{m^3}$). Thus, a small pitch-to-diameter ratio could be permitted for fuel pin bundles cooled by liquid Na, leading to less neutron leakage and less neutron absorption in coolant incurred by small coolant volumetric fraction. A good neutron economy and excellent breeding performance could then be expected; second, as can be observed from Fig 2.4, in a fast spectrum, capture cross sections of Na are small, permitting small neutron losses in coolant inventory; third, the thermal conductivity of liquid Na [21] is around 3 orders of magnitude higher than that of light water [22], leading to a high

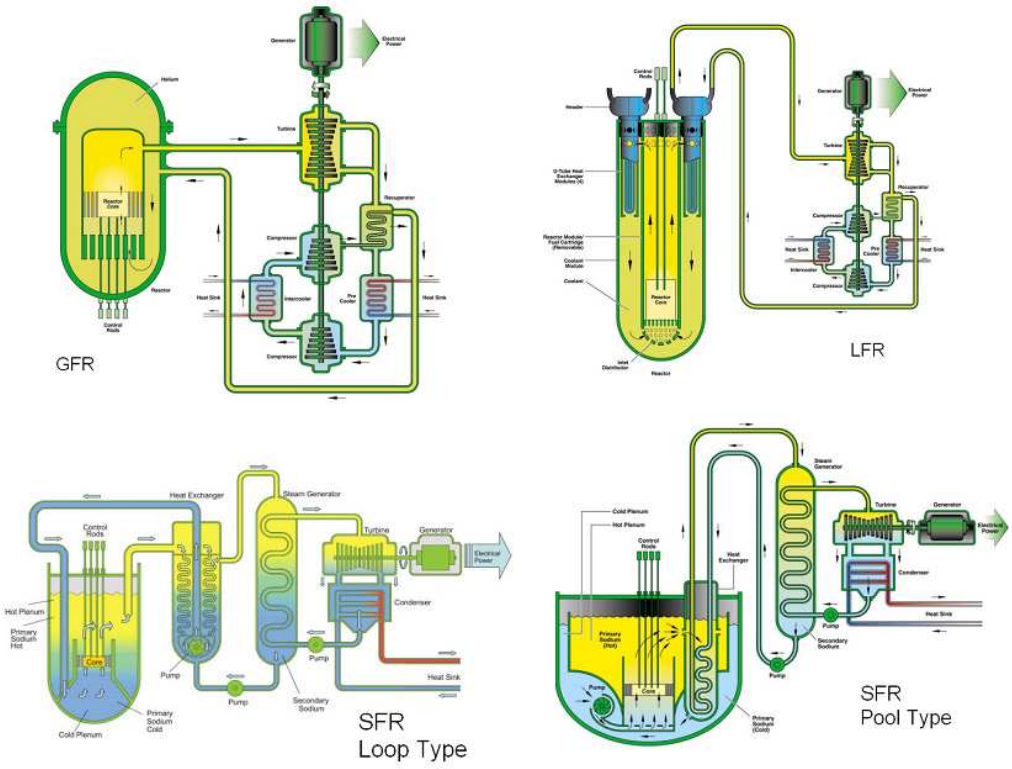


**Figure 2.3.** Different types of fast reactors, [18]

heat transfer coefficient and thus low temperature difference between cladding and coolant for a specific linear power rating.

As a commercialized SFR that has been commissioned since 1980 with the power rating of 1470 MWth (600 MWe) [23], BN600 has excellent operational performance during the last 30 years, permitting proposals to be raised on new fuel loading plans (e.g., UOX/MOX hybrid and full MOX) apart from the reference UOX fuel and new pin configurations (e.g., introducing upper sodium plenum, inner breeding zone) [24] [25]. Moreover, after achieving reliability improvement of primary pump impellers and applying the 20%CW ChS68 stainless steel [26] as cladding material instead of SS316, the lifetime of primary pumps was extended to 35000 $\sim$ 50000 hours and the maximum irradiation damage that the pin cladding can withstand was increased up to 94 dpa [23]. Therefore, the geometrical model of the fully UOX fuelled core specified in the BN600 benchmark, being representative for the medium-sized sodium cooled fast reactors considered in Gen-IV context, was chosen for the studies in Paper **I**.

Although BN600 has a wonderful operational history and more other SFR designs have been promoted by several countries consecutively from 1960s to 1980s [27], SFR technology has not been fully commercialized as LWR technology. On

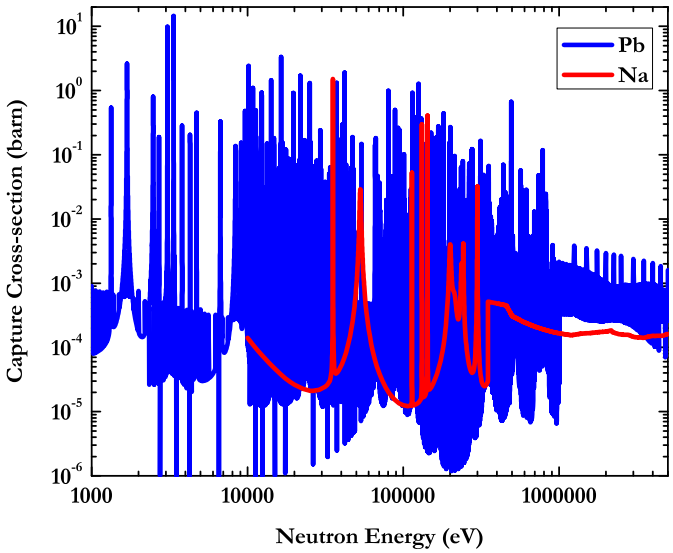


**Figure 2.4.** Capture cross sections of Na and Pb

one hand, except a small rebound during 1975-1980, uranium price stayed at a low level in the past 50 years [28][29], reducing the urgency to widely commission fast reactors aiming at a better usage of uranium resources. On the other hand, there are still several drawbacks to use liquid Na as primary coolant in FRs: first, physical contact between chemical reactive Na and oxide fuel, steam or moisture in air, incurred by cladding rupture, steam pipe break or Na leakage, leads to violent chemical reactions, in the form of fire or explosion, which may turn a small failure to a severe accident as happened in MONJU SFR [30]; second, the boiling point of liquid Na is only 1156 K at 1 atm, leading to a small margin to coolant voiding, which can generate noticeable reactivity response, especially after coolant void worth was enhanced by the introduction of Am. Cladding rupture could also be expected after coolant boils out; third, in order to prevent the leakage of radioactive $^{24}$Na bred from neutron capturing, an intermediate sodium loop is required for a SFR, leading to a more complicated system and higher capital cost; fourth, maintaining 100 K temperature increase from core inlet to outlet, only ≈200 Pa gravity head per meter elevation difference between thermal centers of core and heat exchanger can be generated due to the small thermal expansion coefficient of liquid Na. Thus only a small natural convection flow rate could be expected after the total loss of primary pump head.

### 2.1.2 Lead-cooled fast reactor (LFR)

Comparing to liquid Na, liquid Pb has three major merits: much higher boiling point, larger density change with temperature and inert chemical property with respect to water.

At 1 atm, the boiling point of liquid Pb is equal to 2038 K, which is about 800 K higher than that of liquid Na. Actually, this boiling point is even much higher than creep rupture limits of most cladding materials, which makes liquid Pb boiling no longer an issue during accidental situations.

Correlations to express densities of liquid Pb [31] and liquid Na [21] as a function of temperature are:

$$\begin{aligned} \rho_{Na}(kg/m^3) = &\quad 1012 - 0.2205T(K) - 1.923 \times 10^{-5}T(K)^2 + 5.637 \times 10^{-9}T(K)^3 \\ \rho_{Pb}(kg/m^3) = &\quad 10587 - 1.2220(T(K) - 600.6) \end{aligned} \tag{2.3}$$

From Eq. 2.3, it can be noticed that the density of liquid Pb has a higher decrease than liquid Na for a unit temperature increase, leading to a higher natural convection driven by a unit elevation change between thermal centers in core and heat exchanger. Based on simulations performed by Maschek [32] and Zhang [33], approximately 40% residual flow could be expected for a liquid Pb cooled core, but only less than 5% residue flow could be generated in a typical BN600 type SFR after a total loss of primary pump head.

Unlike Na, liquid Pb is chemically inert to $H_2O$ and steam. Thus, the steam generator could be installed inside the primary loop for LFRs, leading to a compact system and less capital cost for power plant construction.

Thanks to the lower boiling point comparing to liquid Pb, permitting reactors to work at a lower temperature level and thus leaving a bigger margin to clad failure, LBE alloy was first promoted. However, concerning accumulation of highly radioactive $^{210}$Po from neutron capture of $^{209}$Bi in LBE under neutron irradiation, recently, pure liquid Pb cooled BREST reactor and compact STAR-LM reactors were proposed by Russia and US. In the 6th Framework program, design work was performed on a 400 MWth grade ADS design (known as EFIT-400) and a 600 MWe (1500 MWth) grade reactor design (known as ELSY), which are also cooled by liquid Pb [36] [37].

However, until now, no civilian lead-cooled reactors have been commissioned. A major problem when operating continuously at full power is corrosions on cladding and inner structure materials incurred by inter-granular penetration and mass transfer [38], especially for austenitic stainless steels with high concentrations of Ni, which has the highest solubility into liquid Pb comparing to other elements in stainless steel matrix. The mass transfer from stainless steel to liquid Pb may lead to changes of the microstructure, composition, and surface morphology of the structural materials, affecting physical and mechanical properties of the structural materials, e.g., embrittlement and drop of rupture strength. However, it was also found that this corrosion attack can be minimized if a thin protective oxide layer (2-3 $\mu$m) could be

formed on the steel surface [36]. In liquid Pb, the minimum oxygen concentration required for the formation of protective oxide layer on surfaces of Fe-based alloys, equivalent to the oxygen potential ensuring the conditions to form the least stable oxide ($Fe_3O_4$), can be calculated from Eq. 2.4, which is valid in the temperature region from 603 to 1183 K [34][39].

$$\begin{aligned} logC_{\mathrm{Fe,wt.\%}} = &\quad 0.34 - \tfrac{3450}{T} \\ logC_{\mathrm{O,min,wt.\%}} = &\quad -0.75 logC_{\mathrm{Fe,wt.\%}} + 2.355 - \tfrac{10600}{T} \end{aligned} \tag{2.4}$$

The upper limit of oxygen concentration in liquid Pb could be defined by Eq. 2.5, concerning coolant contamination by PbO, which is the most stable lead oxide in solid phase. The accumulation of PbO may clog the coolant flow channel or deposit on heat exchanger surfaces, leading to a loss of cooling capacity. [34].

$$logC_{O,max,wt.\%} = 3.2 - \tfrac{5000}{T} \tag{2.5}$$

Another factor that needs to be considered is that the temperature at the interface between cladding and Pb coolant is not equivalent to the bulk temperature of liquid Pb in order to permit heat transfer from fuel pin to coolant and from coolant to pipes in heat exchanger. If we assume the core inlet temperature equalling 673 K, core outlet temperature equalling 773 K, cladding temperature at hot spot equalling 823 K and pipe wall temperature at the cold spot in heat exchanger equalling 573 K, the allowable oxygen concentration can then be determined as the shaded area in Fig. 2.5. It can be noticed that this area is fairly small, leading to the requirement of a precise oxygen control. Even with oxygen control, stability of the protective oxide layer was reported to be deteriorated if it was exposed HLM flow with a velocity higher than 1.9 m/s [40], which sets the upper limit of liquid Pb flow velocity in LFRs.

### 2.1.3 Gas-cooled fast reactor (GFR)

The typical coolant used in a GFR is He. Unlike liquid Na or liquid Pb, He, being a non-active gas, is chemically and physically compatible with air, moisture and Fe-based alloys, permitting the usage of a direct Brayton gas turbine cycle, by which a higher thermal efficiency could be expected [41]. Besides, since He is already in gas phase at normal operating temperature, coolant boiling or reactivity response from coolant voiding may not be issues any more, providing a better safety performance and also permitting more than 3 times bigger temperature increase from core inlet to outlet comparing to SFRs and LFRs.

Current GFR researches are mainly based on design processes and operational experiences of several graphite-moderated thermal spectrum gas-cooled reactors, e.g., AVR (Germany), HTTR (Japan), HTR-10 (China), and design studies of fast spectrum gas-cooled reactors, e.g., GCFR (US & EU) and the Allegro reactor. These researches are mainly on selecting a proper fuel form, material for cladding and core configuration to provide efficient conversion of fertile U and a better management

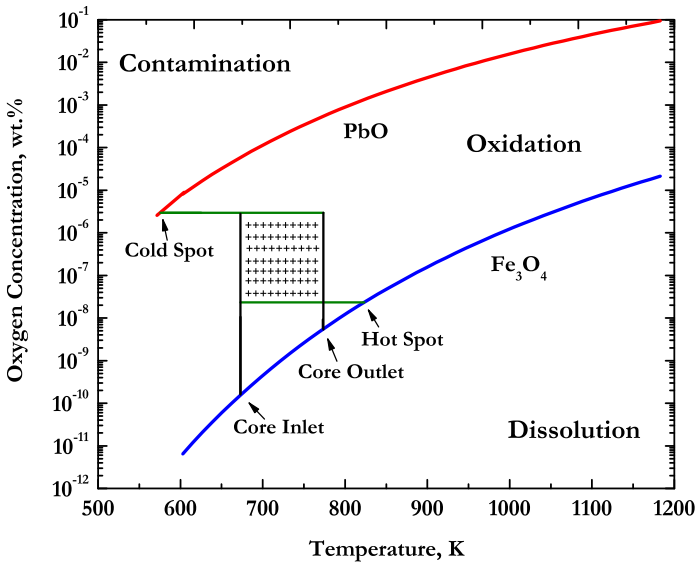


**Figure 2.5.** Oxygen Specifications in liquid Pb

of transuranic inventories, preserving system integrity and compatibility [42]. The conceptual design of a prototype Allegro reactor with a capacity of 50-80 MWth is planned to be accomplished by 2019 and commissioned by 2025 according to R&D plans [43].

Before achieving these targets, there are still some technical challenges need to be faced. First, the radiation resiliency of candidate fuel forms, e.g., actinide-carbide and ceramic-ceramic, for GFR operating conditions (1673 K, 20%h.a. burnup and 150 dpa irradiation dose) should be further investigated [42]. Second, although advanced ceramic materials have been promoted for in-vessel structure usage, their capabilities to withstand temperatures up to 1873 K and fast neutron damage still need to be validated. Third, as can be noticed from Eq. 2.2, the heat removal rate is linearly related to coolant temperature increase ($\Delta$T), cross-sectional area of coolant flow channel (A), coolant velocity (v), coolant heat capacity (Cp) and coolant density ($\rho$). $\Delta$T is limited by material reliability. A is restricted by the concern of neutron leakage and neutron economy. v is limited by the concern of erosion on in-vessel structure with the existence of impurities and Cp of He was reported to be constant in a wide temperature range [44]. Hence, in order to achieve a higher cooling capability, He density should be increased by enhancing coolant pressure in GFR system (normally $\geq$4 MPa [45]). Since He density will intensively decrease according to Eq. 2.6 during depressurization [44], either active blowers that can provide backup pressure or a guard vessel should be implemented to maintain

sufficient cooling capability for decay heat removing.

$$\rho_{\mathrm{He}}(kg/m^3) = 48.14 \times \frac{P(atm)}{T(K)} \times [1 + 0.4446 \times \frac{P(atm)}{T(K)^{1.2}}]^{-1} \tag{2.6}$$

## 2.2 Accelerator driven system

Since the consumption rate of MA will increase with the fraction of MA in fuel for fast reactors, the maximum allowable content of MA should be determined in order to maximize the transmutation capability of fast reactors. However, investigations have shown that loading FRs with only MA inventory, may lead to safety-related problems due to degradations of safety parameters incurred by the absence of fertile U. Besides, higher content of MA, especially Am, may lead to further degradations of safety parameters, such as a reduction of effective delayed neutron fraction, a reduction of the Doppler constant and an increase in coolant void worth [46]. Therefore, the maximum allowable fraction of Am homogeneously loaded into SFRs has been investigated and first quoted as 2.5% [47]. Recently, this limit has been uplifted to 5% for SFRs loaded with metallic fuels [48]. If target sub-assemblies were introduced, this limit for target sub-assemblies may be higher [49].

LFRs are more robust systems than SFRs, regarding core safety during transients, thanks to its high boiling point and excellent natural convection behavior. Thus, up to 10% MA, equivalent to 7% Am, was claimed to be acceptable for a medium LFR with 600 MWe power rating without considering core performances during transients [50]. For a 2400 MWth grade GFR, only 1.1% of MA was proposed to be loaded, corresponding to self-recycling [51]. Hence, in order to host higher fraction of minor actinides aiming at higher MA transmutation rates, FRs should be designed to operate in a sub-critical mode, which can provide improved flexibility and safety characteristics, concerning degradation of core safety performance incurred by minor actinides introduction. The sub-critical core needs to be driven by an external neutron source. In order to generate sufficient neutrons from spallation reactions, the proton beam should be accelerated before bombarding an heavy metal target, giving rise to the term the terminology "Accelerator Driven System (ADS)".

Before further investigations, a terminology named "the energy gain (G)", equalling the ratio of the total power of system ($\mathrm{P}_{tot}$) to the proton beam power ($\mathrm{P}_{acc}$), should be introduced in order to parameterize the influence from changes of target and core designs on power amplification of system. The energy gain of ADS can be calculated by Eq. 2.7, in which $\mathrm{k}_{eff}$ is the multiplication factor of system, $\mathrm{E}_f$ is the averaged energy released per fission reaction, $\nu$ is the fission yield, $\mathrm{E}_p$ is the proton beam energy and $\psi^*$ is the proton source efficiency [52].

$$G = \frac{P_{\mathrm{tot}}}{P_{\mathrm{acc}}} = \frac{k_{\mathrm{eff}}}{1 - k_{\mathrm{eff}}} \frac{E_{\mathrm{f}}}{\nu E_{\mathrm{p}}} \psi^* \tag{2.7}$$

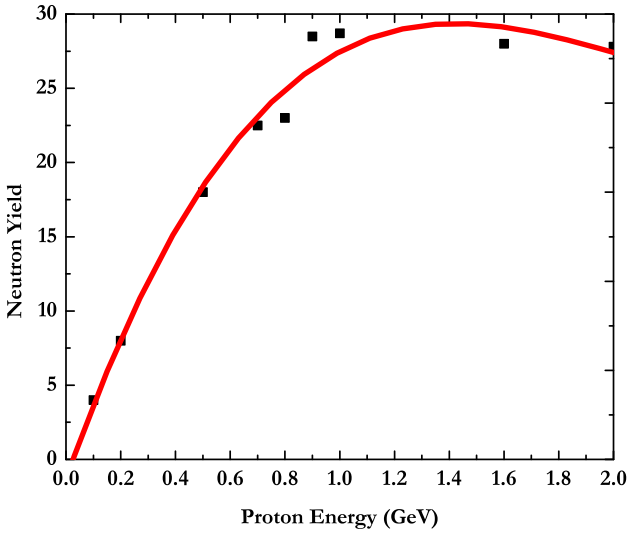


**Figure 2.6.** Neutron yield per proton per GeV for a liquid Pb target with 20 cm radius and 60 cm length

Thus, in order to maximize the energy gain aiming at a better system economy, $k_{eff}$, $\nu$, $E_f$ and $\psi^*$ should be maximized and $E_p$ should be minimized. Since $k_{eff}$ is limited by safety concerns, $E_p$ affects the spallation neutron yield, $\nu$ and $E_f$ are assumed to be constant for a specific fuel composition, the energy gain could be increased by optimizing the system design aiming at a higher $\psi^*$.

### 2.2.1 The accelerator

Spallation neutrons are produced by (p,xn) reactions in spallation target. Fig. 2.6 shows the neutron yield per proton per unit proton energy as a function of incident proton energy for a liquid Pb target with 20 cm radius and 60 cm length [53]. It can be noticed that the neutron yield from (p,xn) and (n,xn) reactions per unit proton energy in spallation target increases with incident proton energy up to around 1.0 GeV. However, the capital cost for construction and maintenance of proton accelerator may continue to increase with proton energy. Besides, the region where source neutrons release may be wider than the core height in the axial direction if higher proton beam energy was applied, leading to higher neutron leakage and thus lower neutron economy. Therefore, 1.0 GeV may be considered as the most suitable proton beam energy.

Current proton accelerators can be categorized into circular accelerators (e.g., cyclotrons, synchrocyclotrons) and linear accelerators (LINAC). For simple cyclotrons, the energy of particle beam is limited under 15 MeV due to a mismatch

between the increase of circulation radius and particle speed or the preset radio frequency. For synchrocyclotrons, due to the variation of frequency and the oscillation of voltage supply, only limited number of particles owning the maximum energy at the outermost region of magnetic field can be captured, which sets the upper limit to the intensity of output beam. Comparing to circular type accelerators, a linear accelerator was reported to be able to deliver a 10 mA/1.0 GeV ion beam with a high reliability, being able to run an EFIT-400 type ADS along [54].

### 2.2.2 The spallation target

#### Target material

Until now, LBE, Hg and liquid Pb have been proposed for high power spallation targets thanks to their excellent performance for source neutron production (high neutron yield per incident proton) and high heat removal capacity ($\rho C_P$). Concerning evaporation of target materials and volatilization of spallation products when connecting to a vacuum cavity required by accelerators, a window was once recommended for spallation target to separate the vacuum cavity and the spallation zone. However, harsh working conditions, including high working temperature, HLM corrosion and irradiation defects, may lead to a target window failure due to accumulations of thermal, irradiation and mechanical loads [55]. A windowless target was then proposed as shown in Fig. 2.7. However, adequate pumping capacity is required to maintain the high vacuum condition above target surface and prevent impurities invasion from target zone into proton beam line. LBE and Pb are then more suitable for a windowless target usage rather than Hg, thanks to their four orders of magnitude lower vapor pressure at the normal operating temperature [56].

#### Target size

Since the fast fission threshold of Am and other fertile nuclides is in the region 0.5-1.0 MeV as shown in Fig. 1.2, inelastic scattering in liquid Pb in target block reduces neutron energies below the region where they may fission fertile nuclides, leading to smaller proton source efficiency [52]. Thus, the spallation target size should be minimized, preserving sufficient heat removal capability. In the suggested ADS design, thanks to the employment of nitride fuel, smaller pin pitch and compact spallation target, the proton source efficiency could be enhanced by 80% comparing to the reference EFIT-400 design. Thus, the proton current and proton beam power required for the system could be reduced by 67% [58], leading to less deposit heat into spallation target, which permits the reduction of spallation target size.

### 2.2.3 The subcritical core

Similar to critical reactors, the sub-critical core in ADS also consists of sub-assemblies, which is in hexagonal geometry in order to achieve better radial power profile and enable a better fit of the spallation target. However, since the safety of sub-critical

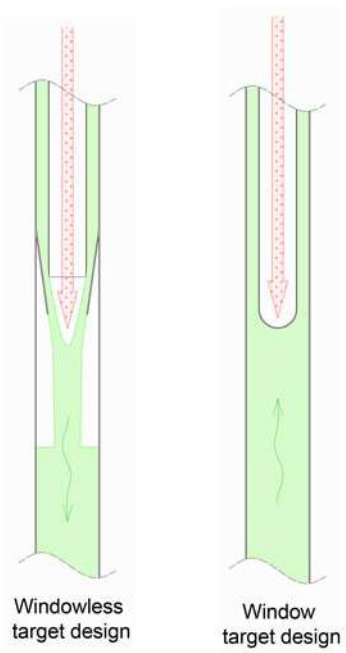


**Figure 2.7.** Window and windowless targets [57]

core can be enhanced due to the bigger margin to prompt criticality than critical facilities, higher minor actinides concentration, can be permitted. In the reference EFIT-400 design, U-free oxide fuel containing 54.3 at.% minor actinides was proved to be allowable, providing a MA consumption rate of ≈42 kg/TWh$_{th}$ [59].

Since the melting point of LBE (44.5%Pb-55.5%Bi) (397 K, at 1 atm) is around 200 K lower than that of Pb, it is used as the primary coolant instead of liquid Pb for the nitride fuelled ADS investigated in Paper **II** aiming at a lower coolant temperature at core inlet, which limits thermal loading and corrosion effect on cladding and in-vessel structures. However, severe inter-granular penetration and mass transfer have also been reported for stainless steel in LBE, leading to the requirement of oxide protective layer as the case for liquid Pb. The minimum oxygen concentration required for the formation of protective oxide layer on surfaces of Fe-based alloys can be calculated from Eq. 2.8, which is valid in the region from 823 to 1053 K. Concerning coolant contamination incurred by PbO accumulation, the upper limit of oxygen concentration in liquid Pb could be defined by using Eq. 2.9, which is valid in 673 - 973 K. Therefore, oxygen control is also required for a LBE-cooled system.

$$\begin{aligned} logC_{\mathrm{Fe,wt.\%}} &= 2.01 - \tfrac{4380}{T} \\ logC_{\mathrm{O,min,wt.\%}} &= -0.75 logC_{\mathrm{Fe,wt.\%}} + 1.2375 - \tfrac{9757}{T} \end{aligned} \tag{2.8}$$

$$logC_{\mathrm{O,max,wt.\%}} = 1.2 - \frac{3400}{T} \tag{2.9}$$

In the nitride fuelled ADS, the pin pitch is reduced from 1.35 cm (for the reference EFIT-400 design) to 1.20 cm in order to reduce the coolant volumetric fraction in system, aiming at a better neutron economy in the sub-critical core. However, since the velocity of LBE flow washing stainless steel bundles is restricted under 1.9 m/s as discussed above, the reduction of pin pitch may lead to reduction of coolant flowrate per pin not only during the normal operating condition but also during transients. In order to maintain an adequate margin to cladding rupture, the austenitic 15/15Ti stainless steel with enhanced thermal and irradiation creep resistance, instead of the ferritic-martensitic T91 stainless steel implemented in the reference EFIT-400 design, is used for the ADS design suggested in Paper **II**. The creep performance of austenitic and ferritic-martensitic steels are discussed in more detailed in Paper **I** and **II**.

In this thesis, transmutation performance of SFRs loaded with oxide, metallic and nitride fuels will be compared with that of the new ADS design loaded with nitride fuel. Since Np contributes negligible radiotoxicity in spent LWR fuel comparing to that from Am [11], transmutation of Np was not considered in this thesis. Besides, the concentration of Cm in LWR fuel is only 1/6 of that of Am, which leads to small impact on core safety parameters. Thus, only the upper limit of Am concentration in SFRs loaded with different types of fuels was assessed in Paper **I**, **III** and **IV** by parameterizing the impact from Am introduction on core safety performance, in order to determine the best transmutation performance that can be achieved by SFRs. In order to investigate the safety performance of SFRs and the newly proposed ADS design loaded with nitride fuel during transients, core safety parameters were calculated by performing neutronic calculations based on core design details. The calculated core performance parameters and safety coefficients, accompany with hydraulic dimensions of sections and thermophysical properties of different components in primary loops of reactors, were then modelled into the transient simulation tool for safety analysis. In the following chapter, tools for neutronic calculation and transient analysis are briefly introduced.

# Chapter 3

# Simulation tools

## 3.1 SERPENT Monte Carlo code

In this thesis, the reactor performance parameters and safety-related reactivity coefficients were evaluated by the SERPENT Monte Carlo code (Version 1.1.13), which is based on continuous-energy cross sections from ACE format data libraries. The development of the SERPENT Monte Carlo code started from the program "Probalistic Scattering Game (PSG)" in VTT Technical Research Centre in Finland [60].

The SERPENT geometrical model is created based on universes, similar to traditional Monte Carlo codes, e.g., MCNP and MCB [60]. The universe based geometry model is excellent for constructing two or three dimensional configurations of fuel pins, sub-assemblies or whole reactor core. In order to simplify the geometrical model creation, several in-build geometrical features were provided by SERPENT, such as cylindrical fuel pins with square and hexagonal lattices for LWR configurations, circular cluster arrays for CANDU.

The burnup calculation, being expressed with time or burn rate steps, is realized by solving the Bateman equations with the Transmutation Trajectory Method (TTA). The decay data library JEFF-3.1.1 and the fission yield data library JEFF-3.1 have been used for the burnup calculation.

Comparing to the traditional Monte Carlo codes, e.g. MCNP, the SERPENT Monte Carlo code has two major merits. First, Monte Carlo calculation is accelerated by 5 to 15 times faster thanks to: 1. evenly subdividing the energy grid of cross section data, which reduces the time consumption to find cross sections during transport; 2. combining conventional ray-tracing and delta-tracking methods, which enhances neutron transport calculation efficiency. Second, homogenized few-group constants, e.g. diffusion rates, effective delayed neutron fractions, diffusion coefficients and statistical errors can be obtained directly [61].

## 3.2 SAS4A/SASSYS transient analysis code

The Safety Analysis System (SAS) was initially written by D. R. MacFarlane as a PhD thesis and upgraded by the staff at safety analysis section at Argonne national laboratory in the following years. The major task of this code is to perform deterministic safety analysis of liquid metal cooled reactors, with respect to severe accidents. Thermohydraulic, neutronic and mechanical responses to accidental scenarios are used to define the working status of core and safety performances of fuel, coolant and structure.

In this thesis, transient simulations were performed with the SAS4A/SASSYS code (version 3.1), which has been extensively validated based on experimental data obtained from the TREAT M-series, EBR-II SHRT and GEMS tests [63]. This version of the code is then qualified for licensing liquid metal (e.g., liquid Na, liquid Pb and Pb/Bi eutectic alloy) cooled reactor cores loaded with oxide or metallic fuels, by means of transient accident simulations, such as Loss-of-Flow (LOF), Transient-over-Power (TOP) and Beam Trip (BT).

In the SAS4A code, one or more sub-assemblies having similar thermophysical properties and thermal hydraulic characteristics are represented by one channel. A whole-core model normally consists of several channels. Heat transfer between fuel, cladding and structure is modeled with a two-dimensional (r/z) heat conduction equation. Heat transfer between cladding and coolant is evaluated by simulating thermal-hydraulics of single or two-phase coolant with a one-dimensional non-equilibrium, homogenous coolant flow model in axial direction. Dimensional changes of fuel column, cladding and fuel assembly can be predicted by using models simulating mechanical behavior of materials and models simulating fission products production, as well as release and transportation. Thanks to the implementation of models for other loops than the primary loop, the SAS4A/SASSYS code is able to analyze transients coupled with the loss-of-heat-sink accident.

In SAS4A/SASSYS, the neutronic behavior of reactor core during transients is evaluated by applying the point kinetic model as shown in

$$\frac{dp(t)}{dt} = \frac{\rho(t) - \beta(t)}{\Lambda(t)} \times p(t) + \sum_k \lambda_k \mathrm{c}_k(t) + \mathrm{s}(t) \tag{3.1}$$

in which p(t), $\rho$(t), $\beta$(t), $\Lambda$(t), $\lambda_k$, $\mathrm{c}_k$(t) and s(t) stand for the power, the reactivity, the delayed neutron fraction, the prompt neutron life time, the group-wise decay constants, the group-wise decay precursor fractions and the source term of core as a function of time [63].

The point kinetic model is an approximation to the time-dependent continuous energy diffusion equation. It has been reported that deviations from the usage of this approximation in sub-critical systems is fairly small ($\leq$5.0%). However, it has also been indicated that the precision of the point kinetic model decreases remarkably when approaching criticality, especially in the case of local perturbations, such as single control rod withdrawal [65], due to slower migration of spatial perturbations. However, if non-local perturbation is assumed to be introduced during LOF and

TOP transients, simulation results obtained from the point kinetic model are still considered to be reliable [64].

The net reactivity change during transients d$\rho$(t) could be calculated by summing up reactivity feedbacks from six mechanisms, incurred by programmed/user-defined, the Doppler effect, fuel pin axial expansion, coolant density change, core radial expansion and control rod drive expansion respectively, as listed in Eq. 3.2.

$$d\rho(t) = d\rho_{\mathrm{p}}(t) + d\rho_{\mathrm{D}}(t) + d\rho_{\mathrm{d}}(ax) + d\rho_{\mathrm{coolant}}(t) + d\rho_{\mathrm{re}}(t) + d\rho_{\mathrm{cr}}(t) \tag{3.2}$$

For ADS, since reactivity swing and reactor shutdown could be managed by adjusting spallation neutron source, control rods are not required. Thus, reactivity responses caused by thermal expansion of control rod drive was not considered in transient simulation for the nitride fuelled ADS.

# Chapter 4

# SERPENT and SAS4A/SASSYS models

## 4.1 SERPENT models

### 4.1.1 The oxide fuelled SFR

The geometry of fuel pin, sub-assembly and other core inner structures was adopted from the reference BN600 design fully loaded with UOX as sketched in Fig. 4.1. This core consists of 369 driver sub-assemblies. Each fuel sub-assembly is loaded with 126 fuel pins and one stainless steel rod in center. Pin pitch and sub-assembly pitch is equal to 8 mm and 99 mm respectively [27][66]. Aiming at a small reactivity loss during burnup, 20 at.% Pu was introduced into the MOX fuel for present core design.

In order to parameterize the impact from Am introduction on core safety parameters seperately from Np and Cm, the Am content in fuel was varied from 0.0 wt.% to 10.0 wt.%. The isotopic composition of Pu and Am were obtained from spent fuel discharged from LWR with 50 MWd/kgHM burnup after 5 years of cooling. The isotopic vectors of Pu are listed in Table 4.1. The Am inventory consists of $^{241}$Am (57.58 at.%) and $^{243}$Am (42.42 at.%). These types of Pu and Am were also loaded into SFRs loaded with metallic and nitride fuels, which will be discussed in following parts of this thesis.

**Table 4.1.** Plutonium vectors

| Isotope | Atomic fraction | Isotope | Atomic fraction |
|---|---|---|---|
| $^{238}$Pu | 3.50 | $^{239}$Pu | 52.88 |
| $^{240}$Pu | 23.82 | $^{241}$Pu | 12.90 |
| $^{242}$Pu | 7.90 | | |

The cladding material adopted for BN600 was the Russian austenitic steel ChS68 containing 0.06 wt.% C, 15.9 wt.% Cr, 0.013 wt.% N, 1.6 wt.% Mn, 1.4 wt.% Si, 14.5 wt.% Ni, 0.3 wt.% Ti, 0.03 wt.% Cu, 0.15 wt.% V and 2.2 wt.% Mo. As stated in

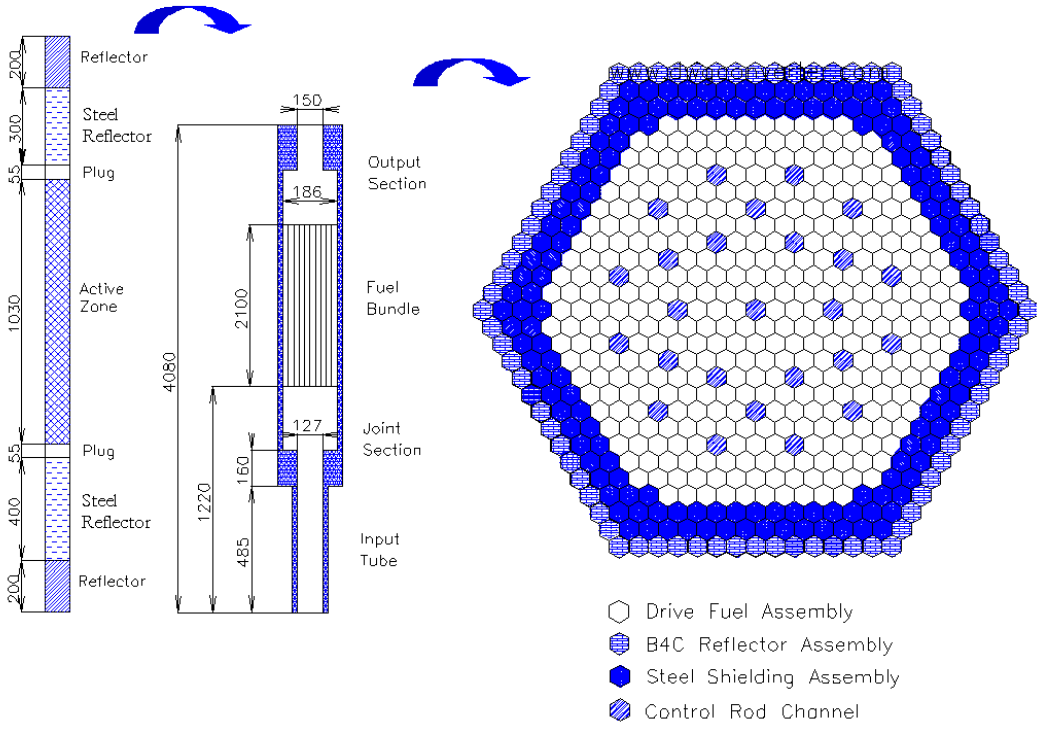


**Figure 4.1.** Geometrical layouts of pin (left), sub-assembly (middle) and core (right) for BN600, in mm [20]

Paper **I**, depleted uranium in axial blankets is replaced by stainless steel, to address the non-proliferation requirement for Gen-IV system. Steel shielding assemblies (SSA) are filled with the ChS68 stainless steel. Boron reflector assemblies consist of pins loaded with $B_4C$, containing 80.0 at% $^{10}B$.

Based on geometrical and compositional details stated above, a 3-D SERPENT model was constructed as shown in Fig. 4.2.

### 4.1.2 The SFR loaded with metallic fuel

For the metallic fuel, the medium sized IFR design with 1575 MWth power rating, being proposed by ANL for the U.S. Department of Energy, was adopted as shown in Fig. 4.3 [67]. In order to achieve a conversion ration equal to unity and maintain the reactivity loss during burnup less than the total shim rod worth, the Pu content in the driver fuel was set at 12.0 wt.%. In order to homogenize the core loading

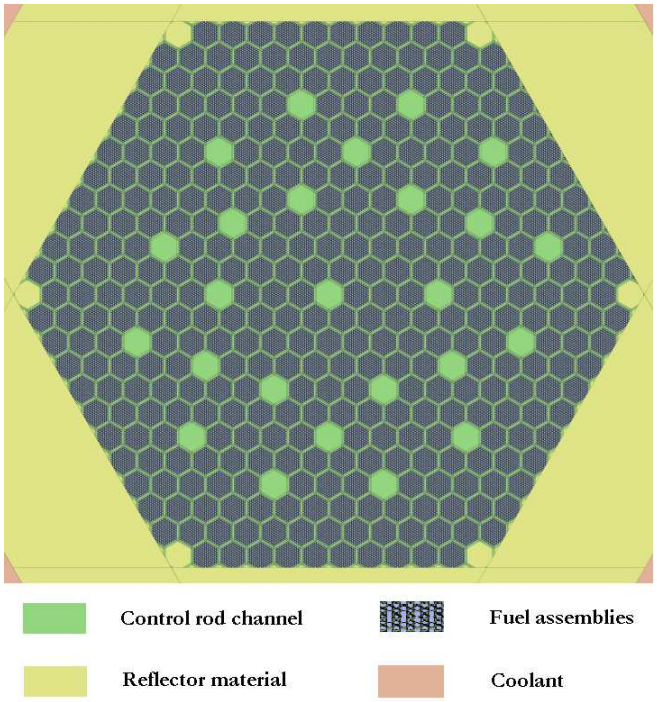


**Figure 4.2.** SERPENT model for the oxide fuelled SFR

in radial direaction and achieve a better neutron economy, steel refector assemblies and $B_4C$ exchange assemblies in the innermost 4 rings, was substituted by driver fuel assemblies with one shutdown rod channel located in core center. Since the core reactivity will be dragged down by the reduction of Pu concentration, the fuel column height was increased from 0.45 m in the reference design to 0.97 m in the present design in order to achieve the required criticality at BOC. Fuel pellet radius was adjusted to provide a 75%TD smear density in order to reduced the cladding strain caused by Fuel-Cladding Mechanical Interaction (FCMI) during burnup [68].

This core consists of 456 driver sub-assemblies. In each fuel sub-assembly, there are 270 fuel pins and one stainless steel rod in array center. Pin pitch and sub-assembly pitch are equal to 8.4 mm and 158 mm respectively [67][20]. Other design details are listed in Table 4.2

The reference cladding material for IFR is HT9, which is a ferritic/martensitic (F/M) steel. The elementary composition of it is listed in Table 4.3.

Based on geometrical and compositional details stated above, a SERPENT model was constructed as shown in Fig. 4.4.

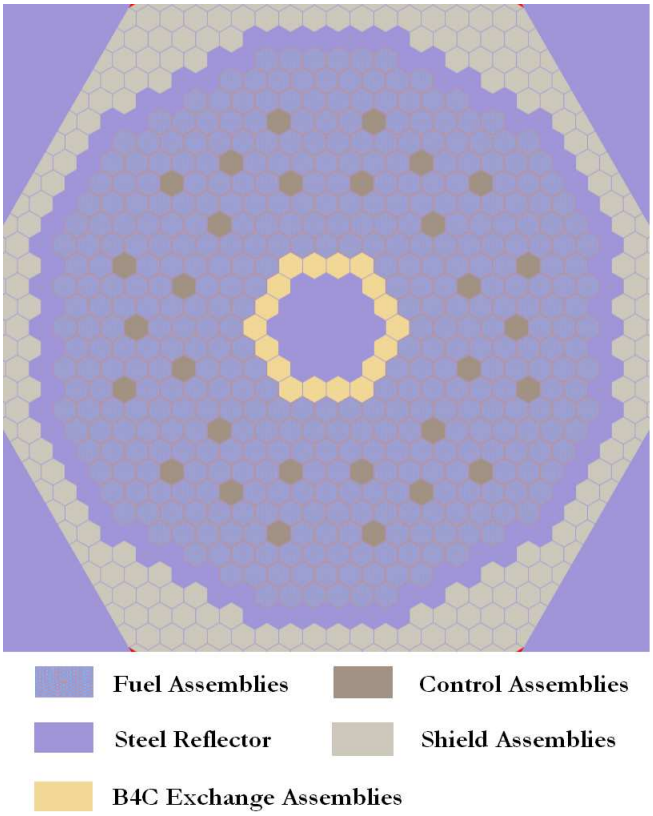


**Figure 4.3.** Core layout of the reference IFR - 1575 MWth burner core

### 4.1.3 The nitride fuelled SFR

The dimensional details of fuel pin and drive fuel assemblies of the representative large-sized SFR loaded with nitride fuel, as listed in Table 4.1, were adopted from the advanced nitride fuel loaded BN1200 core, being proposed by Poplavsky from IPPE [70]. The power rating of the reference BN1200 was set at 2900 $MW_{th}$, providing the power density of 230 $MW/m^3$ and maximum linear power rating of 42 kW/m. The fuel pin pitch and fuel assembly pitch were set at 10.85 mm and 190 mm respectively, permitting 271 pins (270 fuel pins + 1 stainless steel rod) to be loaded into each assembly and 456 driver sub-assemblies to be loaded into core active zone. Fuel pellet radius was set at 7.7 mm in order to provide a smear density of 90% at BOC, which was used for the UN fuel loaded into the BR-10 reactor [20]. Pu content in fuel was increased from 12.4 wt.% to 13.0 wt.% in order to achieve a conversion ratio ∼1.0.

The cladding material used for the nitride core was the D9 stainless steel with the elementary composition listed in Table. 4.5. Depleted uranium in radial blankets is replaced by stainless steel with the same elementary composition as cladding

**Table 4.2.** Dimensions of the SFR loaded with metallic fuel

| Fuel Pin Dimensions | | | |
|---|---|---|---|
| Pellet Diameter | 5.60 | Active Length | 970 |
| Clad I.D. | 6.08 | Blanket Length | 203 |
| Clad O.D. | 7.20 | Plenum Position | Above |
| Pin Pitch | 8.40 | Plenum Length | 800 |
| Reflector Length | 300 | Plug Length | 55 |
| Assembly Dimensions | | | |
| No. of SA | 456 | Nozzle Length | 1220 |
| Flat-to-Flat | 155 | Total Length | 4775 |
| Duct Pitch | 158 | Duct Thickness | 5.18 |
| Head Length | 760 | No. of Pins | 271 |

**Table 4.3.** Elementary composition of the HT9 steel, Fe balanced [69]

| Element | Weight fraction | Element | Weight fraction |
|---|---|---|---|
| Cr | 11.95 | Mo | 1.00 |
| Mn | 0.60 | Ni | 0.57 |
| W | 0.40 | Si | 0.33 |
| V | 0.20 | C | 0.20 |

material, in order to preserve non-proliferation as a requirement of Gen-IV system. Shielding assemblies are loaded with shielding material, containing 10 vol.% $B_4C$ and 90 vol.% concrete. Boron in $B_4C$ contains 80.0 at.% $^{10}B$.

Based on design details stated above, a 3-D SERPENT model could be created as shown in Fig. 4.5.

### 4.1.4 For the nitride fuelled ADS design

The geometry of fuel pins and sub-assemblies loaded into the suggested ADS design was mainly adopted from the reference EFIT-400 design loaded with ceramic-ceramic fuel, except some modifications aiming at a higher neutron source efficiency 4.6 [58]:

1. The spallation target size was reduced from 19 sub-assemblies to 7 sub-assemblies.

2. The number of driver sub-assemblies was reduced from 180 to 78, including 12, 42 and 24 fuel assemblies in inner, intermediate and outer zones respectively.

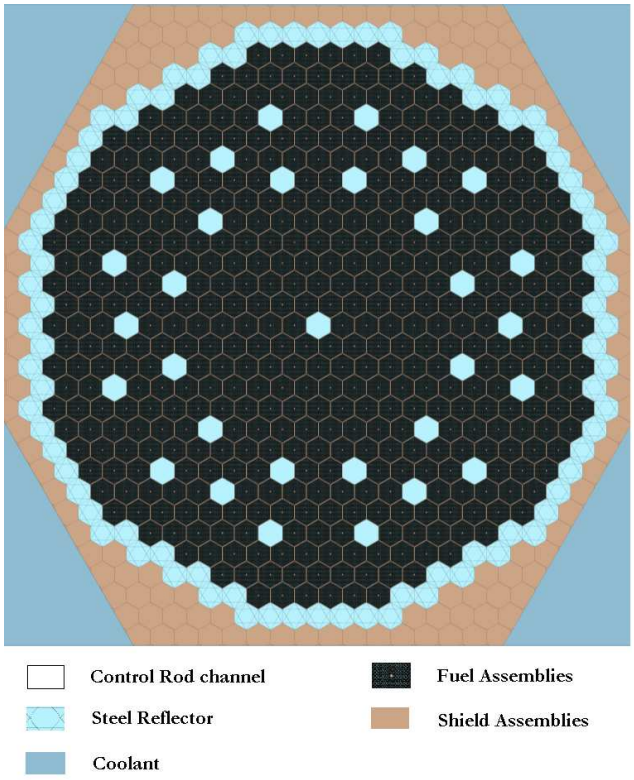


**Figure 4.4.** SERPENT model for SFR loaded with metallic fuel

3. The pin pitch was reduced from 1.35 cm to 1.20 cm, permiting 217 pins (including 216 fuel pins + 1 stainless steel pin in center) instead of 169 pins (including 168 fuel pins + 1 stainless steel pin in center) to be settled in each sub-assembly.

In order to minimize the radial power peaking factor, inert matrix nitride fuel, containing 78.1 vol.%, 73.9 vol.% and 66.1 vol.% ZrN, was loaded into the inner, intermediate and outer zones respectively. The atomic fraction of Pu in HM was fixed to 43.5%. The MA inventory consists of Np (4.0 at.%), Am (91.8 at.%) and Cm (4.2 at.%).

Based on geometrical and compositional information stated above, a SERPENT model for the suggested ADS design was constructed as shown in Fig. 4.7.

## 4.2 SAS4A/SASSYS models

As shown in Fig. 4.8, in the primary loop of the three SFRs studied in Paper **I**, **III** and **IV**, coolant moves from the core to an outlet plenum and then passes through an intermediate heat exchanger (IHX). The primary pump is located at the cold

**Table 4.4.** Dimensions of the nitride fuelled SFR, in mm

| Fuel Pin Dimensions | | | |
|---|---|---|---|
| Pellet Diameter | 7.70 | Active Length | 850 |
| Clad I.D. | 8.10 | Lower Blanket | 400 |
| Clad O.D. | 9.30 | Plenum Position | Below |
| Pin Pitch | 10.85 | Plenum Length | 200 |
| Upper Shielding | 650 | Plug Length | 55 |
| Assembly Dimensions | | | |
| No. of SA | 432 | Nozzle Length | 870 |
| Flat-to-Flat | 181 | Total Length | 3895 |
| Duct Pitch | 190 | Duct Thickness | 3.50 |
| Head Length | 760 | No. of Pins | 271 |

**Table 4.5.** Elementary composition of the D9 steel, Fe balanced [69]

| Element | Weight fraction | Element | Weight fraction |
|---|---|---|---|
| Cr | 13.6 | Ni | 13.6 |
| Mn | 2.10 | Mo | 1.11 |
| Ni | 0.85 | C | 0.40 |
| Ti | 0.30 | | |

leg. In the primary loop of the suggested ADS design, coolant moves from the core to an outlet plenum and then passes through the primary pump and an IHX. The primary pump is located at the hot leg.

The core region in the SAS4A model of the oxide fuelled SFR was subdivided into six different channels loaded with fuel sub-assemblies (including low, intermediate and high enriched zones), steel shielding assemblies, boron shielding assemblies and control rods respectively, which were categorized by different thermophysical properties, neutronic characteristics and power densities. Core regions in the SAS4A model of SFRs loaded with metallic and nitride fuels were simply divided into four channels, including one hottest channel loaded with hottest fuel pins, one average channel loaded with the rest fuel pins, one control rod channel and one channel loaded with shielding assemblies.

The suggested ADS core was represented by 5 channels, including 3 fuel channels stand for three fuel zones loaded with nitride fuels containing different fractions of matrix, 1 bypass channel stands for the spallation target and 1 reflector channel.

The foot and exit section of sub-assemblies are significant components contributing pressure drops, and thus represented by liquid segments called pipes at core inlet and outlet separately as shown in Fig. 4.8. Pressure drops from different parts of

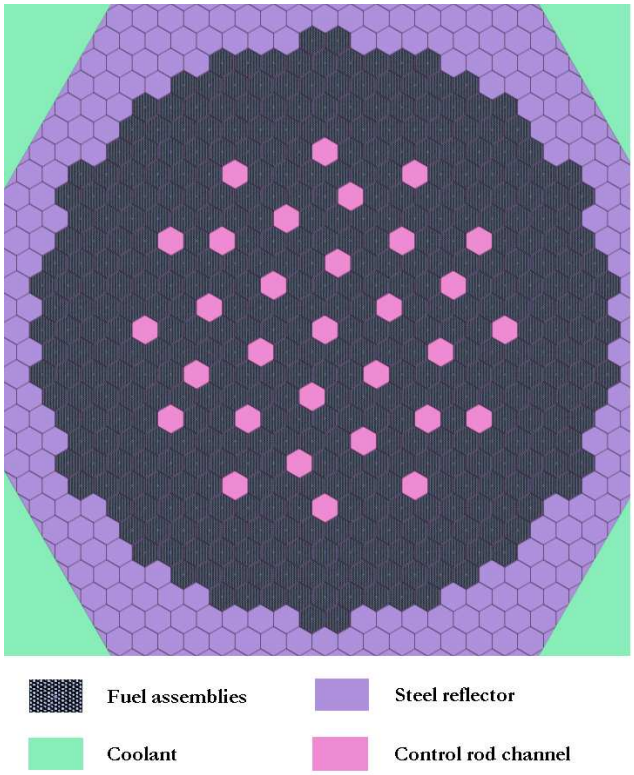


**Figure 4.5.** SERPENT model for the nitride fuelled SFR

assembly foot and exit could then be added to the primary circuit by simply adjusting orifice coefficients of these two pipe segments. Since geometrical details of upper and lower inner structures in studied SFRs needed for pressure drop calculations are not available in open literature, pressure drops through the coolant inlet plenum, the core active region and the coolant outlet plenum are simply assumed to follow the ratio of 0.35:0.50:0.15, which is equal to the one recommended for the EFIT-400 design [71]. Pressure drop through the core region at steady state was set at 0.5 MPa [20] for oxide, metal and nitride fuelled SFRs. For the suggested ADS design, this pressure drop was reported to be 0.032 MPa. Total pressure drop through the primary loop of all three SFRs was set at 2.00 MPa, including $\Delta P_{core}$ (1.00 MPa), $\Delta P_{IHX}$ (0.80 MPa) and $\Delta P_{pump}$ (0.20 MPa), in order to make a consistent comparison. Total pressure drop through the primary circuit of the suggested ADS design is equal to 0.141 MPa, including $\Delta$ $P_{core}$ (0.064 MPa), $\Delta$ $P_{IHX}$ (0.034 MPa) and $\Delta$ $P_{pump+accessories}$ (0.043 MPa), if the coolant velocity was set at 0.80 m/s as recommended for the reference EFIT-400 design [72]. Accessories are components like core diagrids, decay heat removal heat exchangers, fuel handling machines and so on.

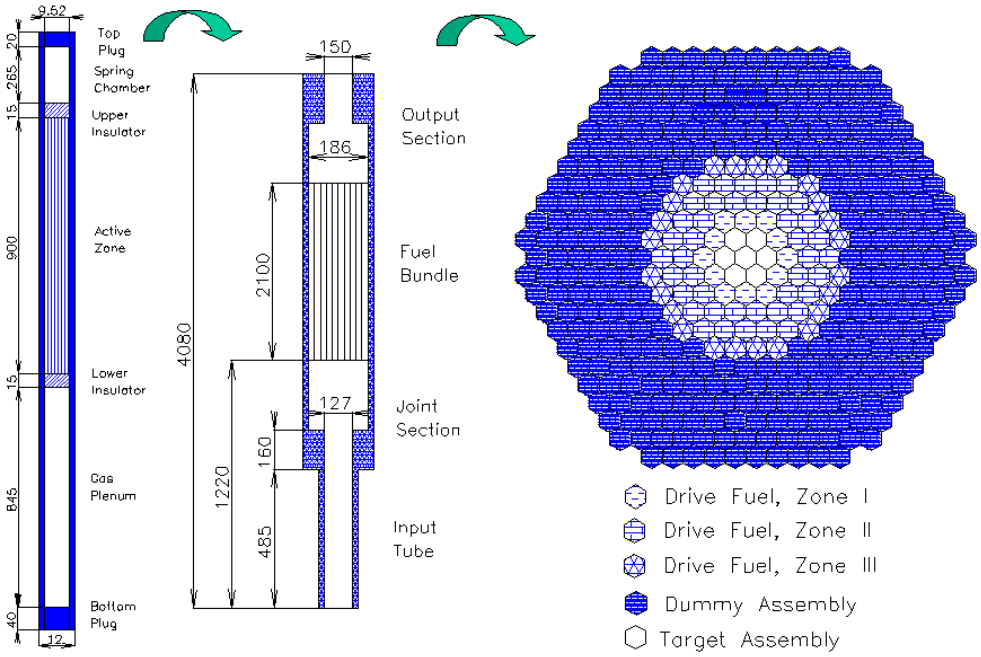


**Figure 4.6.** Geometrical layouts of pin (Left), sub-assembly (middle) and core (right) for the suggested ADS design [32]

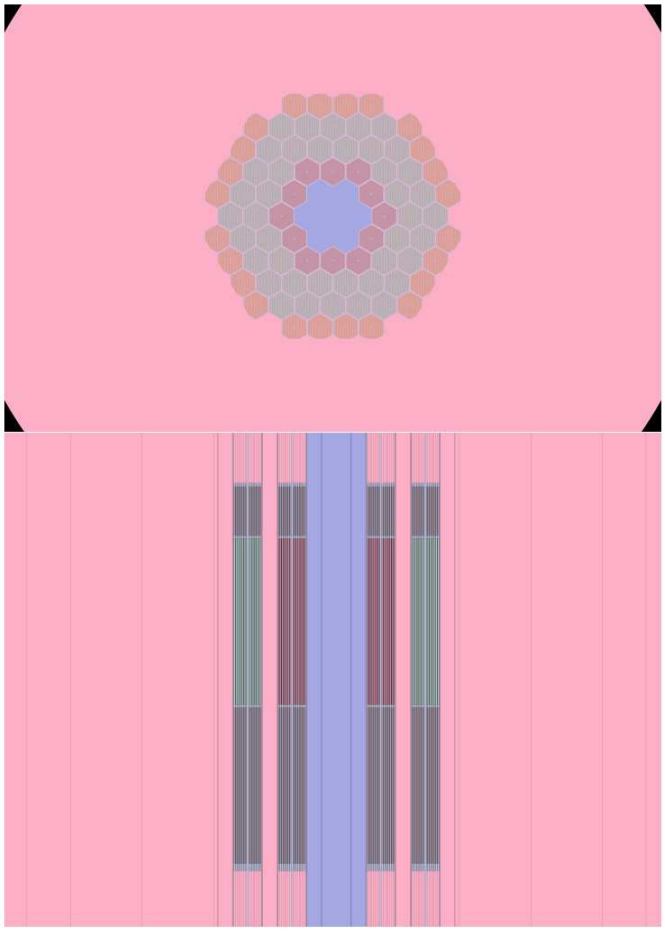

**Figure 4.7.** SERPENT model for the suggested ADS design, top view (above) and side view (below)

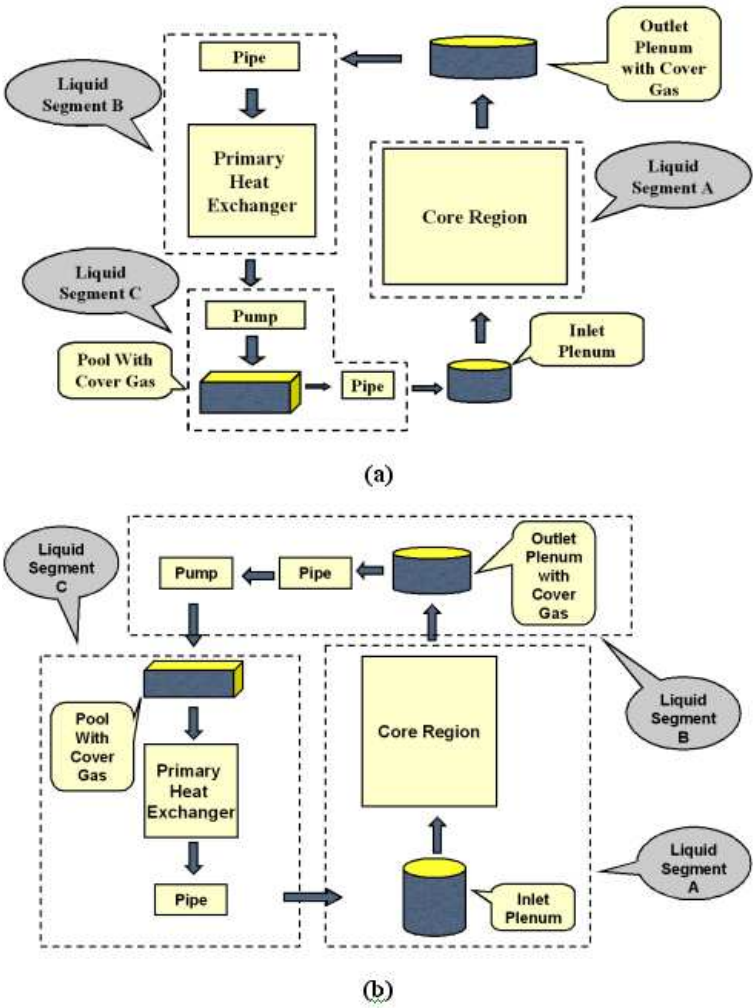


**Figure 4.8.** SAS4A/SASSYS models of SFRs (a) and ADS (b)

# Chapter 5

# Effects from the introduction of americium

For fast critical reactors, the consumption rate of Am is highly dependent on the ratio between Am and Pu in the fresh fuel. A larger Am/Pu ratio permits a higher Am burning rate, in terms of kilogram Am consumed per TWh power produced. However, since Am has a detrimental effect on essential safety parameters of reactor core, e.g. the effective delayed neutron fraction, the Doppler constant, the coolant void worth and the axial/radial expansion reactivity coefficient, a careful analysis of transient performance as a function of Am concentration in the fuel must be performed, also taking the degradation of thermophysical properties into account. Then, the maximum allowable Am content for SFR cores loaded with different types of fuel can be concluded and transmutation efficiencies of SFRs can be compared with that of the suggested ADS. In this chapter, impacts from Am introduction on core safety parameters and thermophysical properties of different fuel types are summarized.

Fresh Am is a white lustrous metal. The melting point and density of pure Am are 1267 K and 13.67 g/cm$^3$ (293 K) respectively [73]. In dry atmosphere, Am metal will be tarnished by heat generated from spontaneous fission reactions and $\alpha$ irradiation.

The first identified Am isotope is $^{241}$Am, which was synthesized from successive neutron capture reactions of Pu by Seaborg et al. at 1944 [74]. Apart from $^{241}$Am, at least 10 Am isotopes with atomic mass ranging from 237 to 247 have been synthesized, in which $^{237}$Am has the longest half-life time equaling 7400 years.

Like other transuranic nuclides with atomic numbers higher than 95, all Am isotopes can undergo $\alpha$ decay and spontaneous fission reactions. $\alpha$ particles released from $\alpha$ decay reactions of $^{241}$Am has the average energy of 5.48 MeV, which is three times higher than those released from $\alpha$ decay reactions of $^{226}$Ra. $\gamma$ particles discharged during $\alpha$ decay and spontaneous fission reactions have the average energy of around 59 keV and 7 MeV [76] respectively. Thus, accumulation of Am nuclides leads to difficulties for fuel handling.

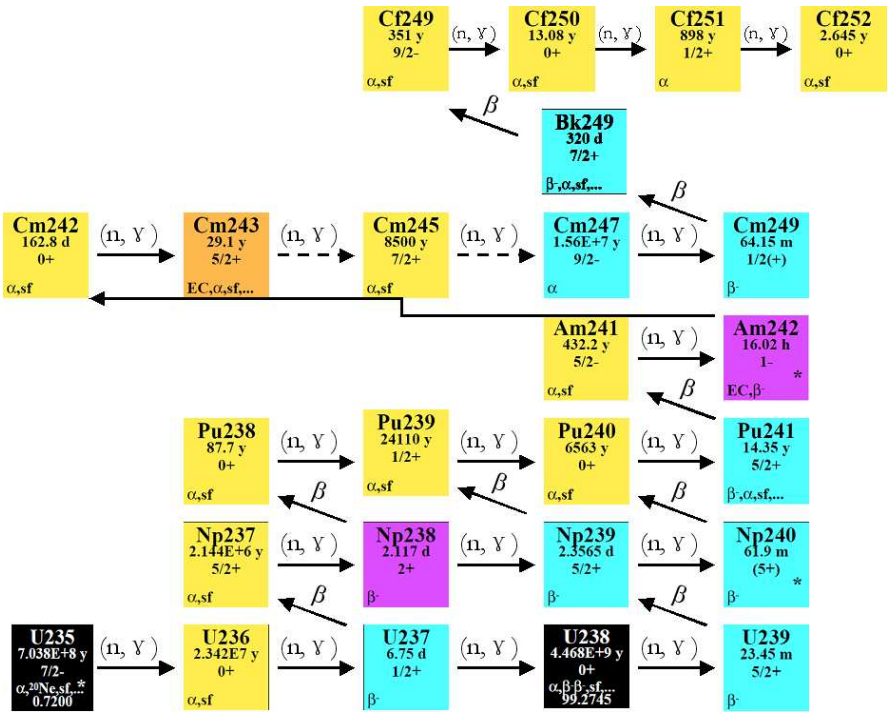


**Figure 5.1.** Relations of the most important actinides, via $\alpha$-decay, $\beta$-decay and neutron capture reactions

Nevertheless, since fission probabilities of the major Am isotopes are close to zero in a thermal neutron spectrum as can be noticed from Fig. 1.2, Am nuclides are more likely to be converted $^{252}$Cf, which is a strong neutron source and heat emitter, instead of being fissioned if they are recycled in a thermal spectrum as shown in Fig. 5.1. It has been reported that the equilibrium concentration in a fast spectrum of Cf and the corresponding neutron reactivity will be 2-3 orders of magnitude lower than in a thermal spectrum. Thus, fast neutron facilities are better suited to implement transmutation of Am [75].

For the suggested ADS design, isotopic composition of fuel and core design parameters have been adjusted to achieve a higher proton source efficiency comparing to the reference EFIT-400 design, preserving the same minor actinide transmutation rate equalling 42 kg/TWh. Thus, in Paper **II**, the major task is to confirm the suggested ADS design by investigating core safety performances during the postulated transients.

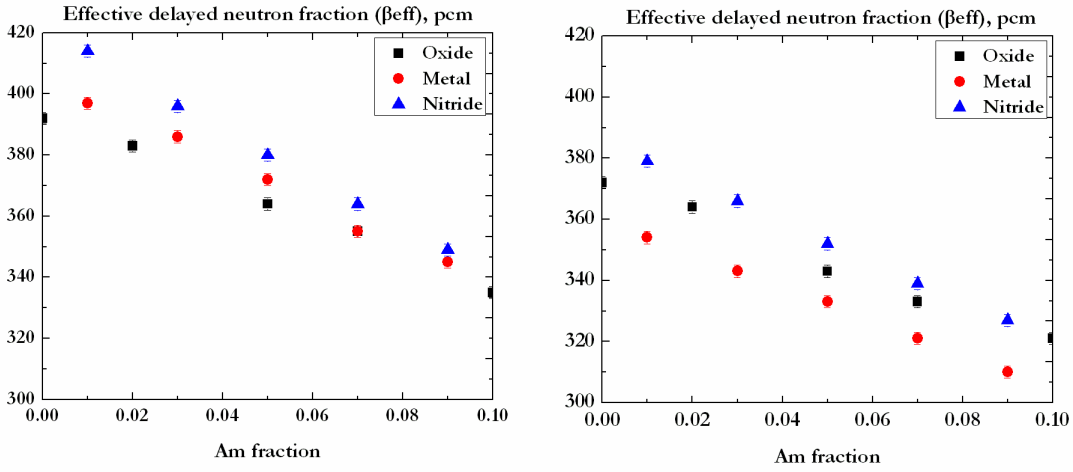


**Figure 5.2.** Effective delayed neutron fraction at BOC (left) and EOEC (right), in pcm

## 5.1 Impacts on core performance parameters and reactivity coefficients

Effects from the introduction of Am on reactivity coefficients and core performance parameters were evaluated by modifying oxide, metallic and nitride fuels with different fractions of Am and then loaded into SERPENT models described in Chapter 4. Results from these neutronic calculations are summarized into Fig. 5.2, 5.3, 5.5, 5.7 and 5.8.

### 5.1.1 For sodium-cooled fast reactors

#### The effective delayed neutron fraction

Neutrons released from fission reactions can be divided into prompt and delayed neutrons. A prompt neutron is a neutron emitted immediately from fission reactions. A delayed neutron is a neutron emitted from fission products decay anytime from several milliseconds (ms) to about 55 seconds (such as $^{87}$Br) [77]. The delayed neutron fraction ($\beta$) is then defined as the number of delayed neutrons divided by the number of total fission neutrons. The effective delayed neutron fraction ($\beta_{eff}$) is defined as the fraction of fission inducing neutrons that were born as delayed neutrons.

Since the capture cross section of $^{241}$Am is 5 times higher than that of $^{238}$U for the average energy of delayed neutrons (≈0.5 MeV), the effectiveness of delayed neutrons will decrease in proportion to Am content as can be noticed from Fig. 5.2. Smaller $\beta_{eff}$ may lead to: first, shorter mean generation time ($\Lambda$) of fission

neutrons, limiting the time for non-malignant responses from either the manual operation or inherent safety characteristics; second, higher sensitivity of core power to reactivity fluctuations according to Eq. 3.1. The decrease of $\beta_{eff}$ during burnup is mainly due to the conversion of $^{238}$U to Am and Pu nuclides with lower $\beta_{eff}$ values, through neutron absorption. The slightly bigger decrease for the metallic fuel from BOC to EOEC is mainly due to the higher burnup level of metal core at EOEC (8.0 at.% HM) than that of BN600 and BN1200, being equal to 6.7 at.% HM.

It can also be noticed from Fig. 5.2 that $\beta_{eff}$(Nitride)>$\beta_{eff}$(Metal)>$\beta_{eff}$(Oxide) for cases with Am content lower than 5.0 wt.%, which is mainly due to the different concentrations of Pu, providing less delayed neutrons.

After introducing more Am, this difference will converge because the degradation effect from Am will partially offset this effect incurred by Pu content differences.

### The Doppler constant

The Doppler effect of fertile nuclides is mainly from the Doppler broadening of capture resonances of $^{238}$U and $^{240}$Pu, permitting more neutrons distributed in a wider energy spectrum to be captured, which leads to a lower effective multiplication factor. The Doppler constant is then used to correlate the reactivity change with fuel temperature change as shown in Eq. 5.1, in which $\rho(T_1)$ and $\rho(T_2)$ stand for core reactivities at fuel temperatures $T_1$ and $T_2$.

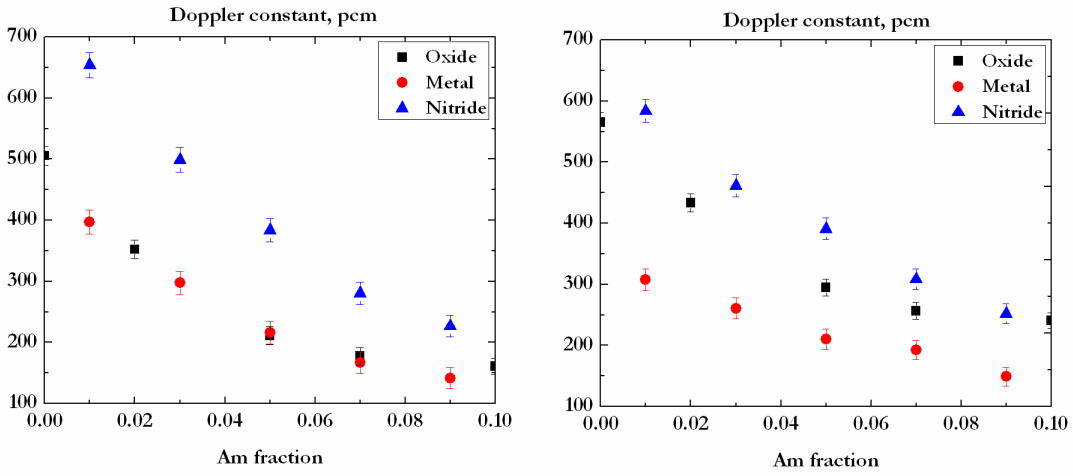


**Figure 5.3.** Doppler constant at BOC (left) and EOEC (right), in pcm

$$K_D = -\frac{\rho(T_2) - \rho(T_1)}{ln(T_2/T_1)} \tag{5.1}$$

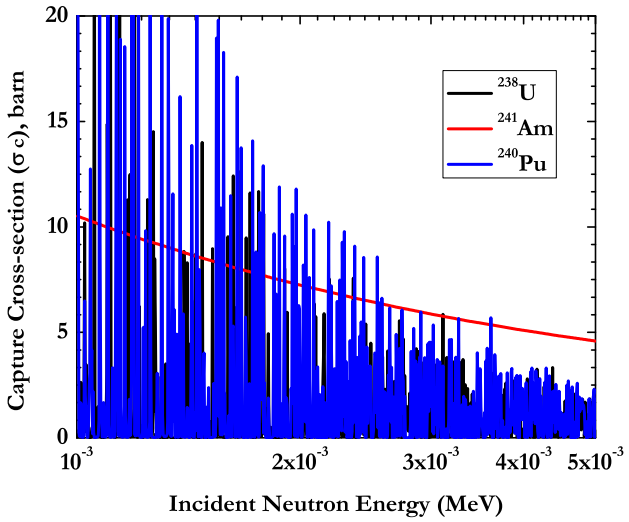


**Figure 5.4.** Capture cross-section spectrums of $^{238}$U, $^{241}$Am and $^{240}$Pu

As can be observed from Fig. 5.3, the Doppler effect will be weakened by more than a factor of two when Am content was increased from 1.0 wt.% to 9.0 wt.%. This is mainly because the introduction of Am permits less fission neutrons to enter the energy region where the Doppler effect is the most efficient. Besides, the Doppler broadening effects of $^{238}$U and $^{240}$Pu are weakened since their resonance capture regions are covered by that of $^{241}$Am as shown in Fig. 5.4, whose Doppler broadening effect is weaker as shown in Fig. 5.5.

For the oxide fuelled SFR, the Doppler constant increases with burnup as shown in Fig. 5.2, which is the consequence of Pu consumption during burnup because the conversion ratio was set at 0.97, being slightly lower than unity. For metallic fuel and nitride fuel loaded SFRs, being operated with conversion ratio equal to unity, the Doppler constants will decrease with burnup mainly due to the conversion from $^{238}$U to Pu and Am nuclides, having weaker Doppler effect.

### The void worth

The coolant void worth is a safety parameter that describes the reactivity change after coolant in core boils out. It can then be calculated by subtracting the reactivity of the voided core from the reactivity during normal operating conditions. Since liquid metal is the primary coolant and functions as neutron reflector, two major impacts may arise from the coolant voiding on core performance: first, neutron flux will be hardened due to less neutron moderation; second, core leakage will be higher due to less neutron reflection.

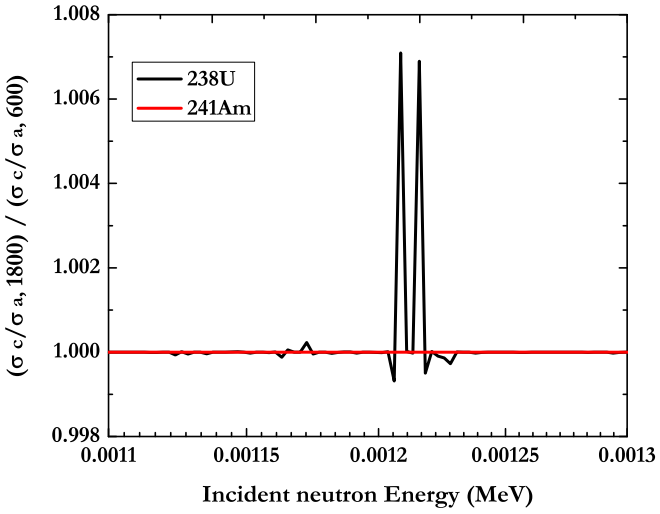


**Figure 5.5.** The increase of capture rate by Doppler broadening

Since fission probabilities of Am nuclides are much higher than that of $^{238}$U and increase with incident neutron energy in the energy region around 500 keV, introduction of Am will lead to a higher sensitivity to the spectral shift of incident neutrons. Thus, for all reactor designs, an almost linear increase of the coolant void worth with Am concentration could be noticed from Fig. 5.6 due to the negligible change of core leakage after coolant voiding. Besides, coolant void worths increase with burnup, which is mainly due to decrease of the ratio between fissile and fertile nuclides during burnup, since fissile nuclides, e.g., $^{239}$Pu and $^{241}$Pu, contribute much less positive void worths comparing to fertile nuclides.

### Radial and axial expansion reactivity coefficients

The radial expansion reactivity coefficient ($\alpha_R$) is a safety parameter that correlates the reactivity change with the radial expansion of sub-assembly diagrids. It can be calculated as $\alpha_R$=$\Delta\rho/\Delta$T, in which $\Delta\rho$ stands for the reactivity change due to a specific diagrid expansion and $\Delta$T stands for the temperature change required to realize this specific diagrid expansion. Similarly, the axial expansion reactivity coefficient, calculated as $\alpha_A$=$\Delta\rho/\Delta$T, is used to correlate the reactivity change with the thermal elongation of fuel pin in axial direction.

It can be noticed from Fig. 5.7 that the radial expansion of sub-assembly diagrid leads to a decrease of core reactivity, which is mainly due to enhanced neutron leakage in axial direction. Moreover, since the introduction of Am hardens the neutron spectrum, the radial expansion reactivity coefficients becomes more negative

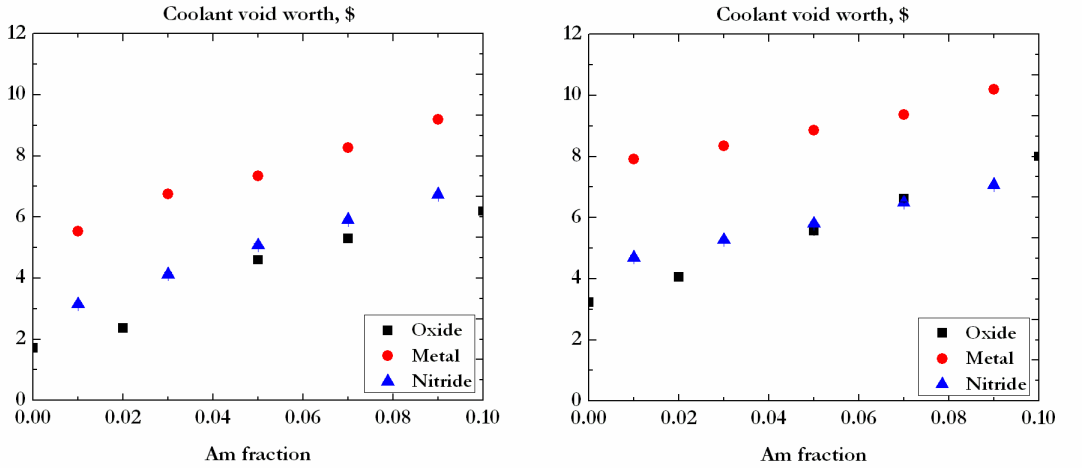


**Figure 5.6.** Coolant void worth at BOC (left) and EOEC (right), in $

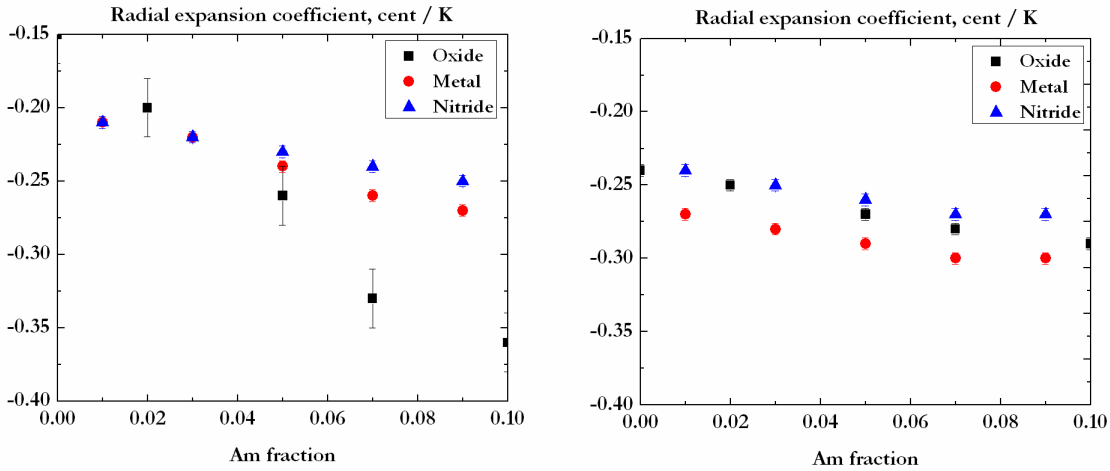


**Figure 5.7.** Radial expansion reactivity coefficients at BOC (left) and EOEC (right), in ¢/K

with the increase of Am content at BOL due to higher neutron leakage in axial direction and lower fission probabilities of Am nuclides for incident neutrons with lower energy incurred by more moderation.

Since the neutron spectrum in the oxide fuelled core is softer than those in metal and nitride fuelled cores due to higher moderation power from oxide atoms, the introduction of Am leads to a stronger impact on neutron leakage and average neutron spectrum for oxide core than metal and nitride fuelled cores at BOC state,

and then on the radial expansion reactivity. At EOEC, due to the accumulation of fission products, functioning as additional moderators, the average neutron spectrum in metal and nitride fuelled cores will be softened and impacts from different Am concentrations become slightly more obvious.

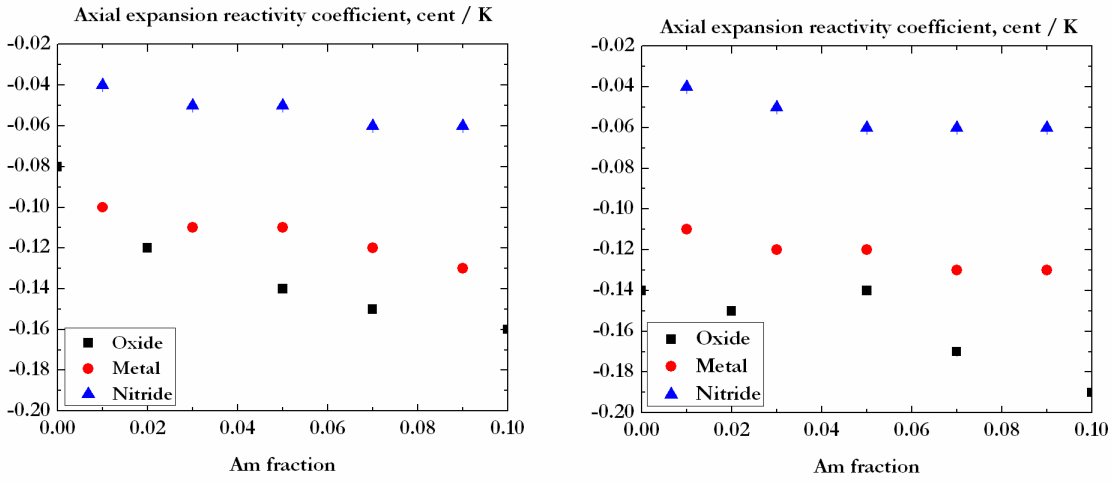


**Figure 5.8.** Axial expansion reactivity coefficients at BOC (left) and EOEC (right), in ¢/K

Since more fissile material moves up and downwards into regions where neutrons are further moderated by coolant in hot pool and cold pool, the axial expansion of fuel pin leads to the reduction of the multiplication factor as shown in Fig. 5.8.

For the oxide fuelled core, the introduction of 10.0 wt.% Am makes the axial expansion reactivity coefficient a factor of two more negative due to a higher sensitivity to the spectral shift of incident neutrons for Am nuclides. Since moderation effects from Zr atoms in metallic fuel and N atoms in nitride fuel are smaller than that from the O atoms in oxide fuel, the impact from the introduction of Am on axial expansion reactivity coefficient is less for IFR and BN1200 designs than that for BN600 design.

### The effective multiplication factor

The effective multiplication factor ($k_{eff}$) is equal to the average number of neutrons produced by one fission reaction that can cause another fission reaction. Except these "effective" neutrons, other fission neutrons will either be consumed by non-fission reactions or leak out from the active region.

It can be observed from Fig. 5.9 that: 1. negative $k_{eff}$ swing could be noticed for most cases due to consumption of fissile materials and generation of fission products, which leads to lower concentration of fissile material in fuel matrix and also more moderation on fission neutrons; 2. $k_{eff}$ swings for IFR and BN1200 are

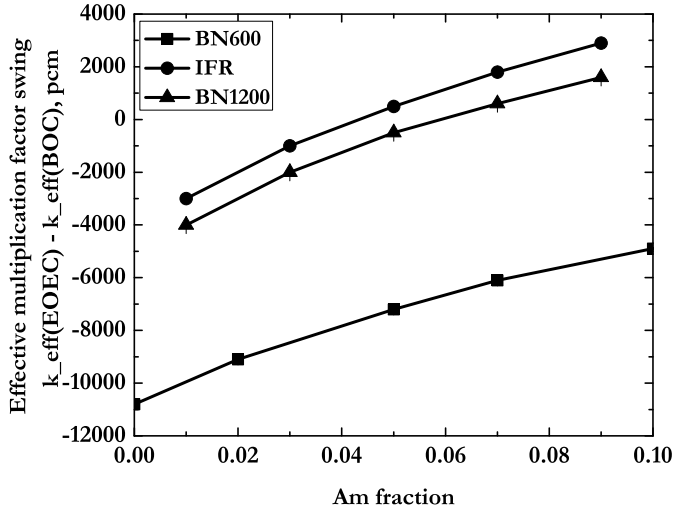


**Figure 5.9.** Effective multiplication factors swings for different Am contents

less than 4000 pcm, being less than the sum of control rod worth, thanks to proper selections of Pu contents aiming at the self-sustainability; 3. $k_{eff}$ swing for cases with higher Am content are smaller than cases with lower Am content or even turn to positive thanks to the transmutation of $^{241}$Am via $^{242}$Cm to $^{238}$Pu and breeding of $^{244}$Cm from $^{243}$Am.

### 5.1.2 Safety parameters of the suggested ADS design

**Table 5.1.** Reactivity coefficients and core performance parameters

| ADS Types | Nitride ADS SERPENT | Nitride ADS MCNP | EFIT-Pb (cermet) | EFIT-Pb (cercer) |
|---|---|---|---|---|
| $k_{eff}, BOC$ | 0.97 | 0.97 | 0.97 | 0.97 |
| $k_{eff}$ swing, pcm | 1780 | 234 | 165 | 709 |
| $\beta_{eff}$(pcm) | 164±2 | 142±13 | 168 | 148 |
| $W_{coolant}$(pcm), BOC | 3322±10 | 3504±18 | 7335 | 7077 |
| $W_{coolant}$(pcm), EOC | 3026±10 | 2877±18 | 6325 | 6037 |
| $K_D$(¢) | 22±6 | 31±5 | 68 | 31 |
| $\alpha_R$(¢/K) | -0.56±0.03 | -0.50±0.05 | -0.64 | -0.54 |

Comparing to the reference EFIT-400 designs, the most important impact in-

curred by the pin pitch reduction from 1.35 cm to 1.20 cm is reported to be a ≈50% decrease for coolant void worth as shown in Table 5.1, thanks to the smaller volumetric fraction of coolant. Since Am is the major contributor to positive coolant void worth, the coolant void worth decreases by around 10% during burnup due to the consumption of Am.

## 5.2 Effects on major thermophysical properties

### 5.2.1 Thermal conductivity

**Oxides Fuel**

$AmO_2$ and $Am_2O_3$ are the most stable americium oxides, having Face Centered Cubic (FCC) and Hexagonal Closed Packing (HCP)/Body Centered Cubic (BCC) crystal structures respectively [78]. The molar ratio between these two oxides is affected by temperature and oxygen potential, determining the stoichiometry deviation of oxygen (x) in $AmO_{2-x}$.

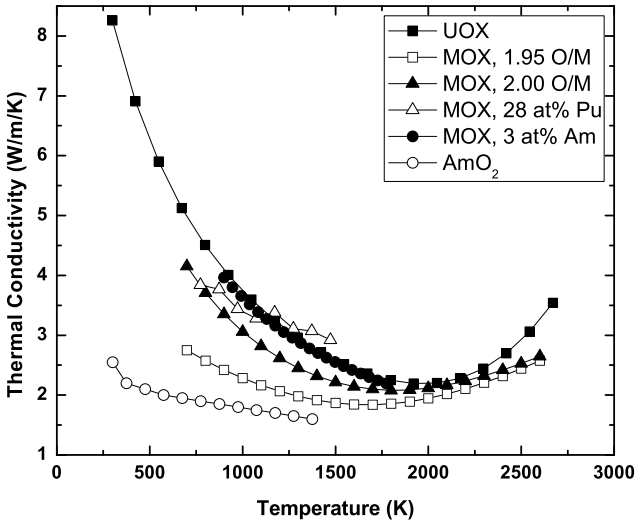


**Figure 5.10.** Thermal conductivities of actinide oxides

Thermal conductivities of different oxides are compared in Fig. 5.10, from which it can be noticed that:

- Thermal conductivity of $AmO_2$ [79] is more than 50% lower than that of $UO_2$ [80].

- If the stoichiometry deviation of oxygen was set at 0, the introduction of less than 28 at.% Pu or less than 3 at% Am gives negligible impact on thermal conductivity of $UO_2$ [81] [82] [83] [80] [84].

- Thermal conductivities of actinide oxides are sensitive to the stoichiometry deviation of oxygen. This effect can be expressed using correlation 5.2, in which x stands for the stoichiometry deviation of oxygen, being set at 0.05 for the MOX fuel investigated in Paper **I**, and t is equal to T/1000 [81].

$$\begin{aligned} A &= 2.85x + 0.035 \\ C &= -0.715x + 0.286 \\ k_{MOX} &= 1.158(A + Ct)^{-1} + 6400\frac{e^{-16.35/t}}{t^{5/2}} \end{aligned} \tag{5.2}$$

Four phenomena were suggested to be considered in order to estimate the burnup effects on thermal conductivity of $UO_2$ [86], which were assumed to be valid for fuels in this thesis study:

- Dissolution and precipitation of solid fission products ($\kappa_d$)
- Fission gas bubbles and pores ($\kappa_p$)
- Stoichiometric deviation ($\kappa_x$)
- Radiation damage induced circumferential cracks ($\kappa_r$)

$\kappa_d$ and $\kappa_p$ are dependent on the burnup and could be expressed into Eq. 5.3 and Eq. 5.4, in which T is in Kelvin and B is in at%.

$$\begin{aligned} \omega &= 1.09\ B^{3.265} + 0.0643(T/B)^{1/2} \\ \kappa_d &= \omega[arctan(1/\omega)] \end{aligned} \tag{5.3}$$

$$\kappa_p = 1 + \frac{0.019B}{(3 - 0.019B)[1 + e^{-(T-1200)/100}]} \tag{5.4}$$

**Actinide nitride and nitride composite(Ac,Zr)N**

Thermal conductivities of different actinide nitrides were compared in Fig. 5.11, based on correlations proposed by Arai [87], Basini [88] and Nishi [103] respectively. It can be noticed that thermal conductivities of UN, NpN and PuN are around 150%, 60% and 30% higher than that of AmN. The introduction of 75 at% ZrN, being a chemical stablizer with high thermal conductivity, increases the thermal conductivity of (Pu,Zr)N by more than 80% [88]. Hence, thermal conductivity of AcN and (Ac,Zr)N can be simply calculated by using Vegard's law as expressed in Eq. 5.5, in which c and k stand for atomic fractions of actinides in fuel and thermal conductivities of different actinide nitrides respectively.

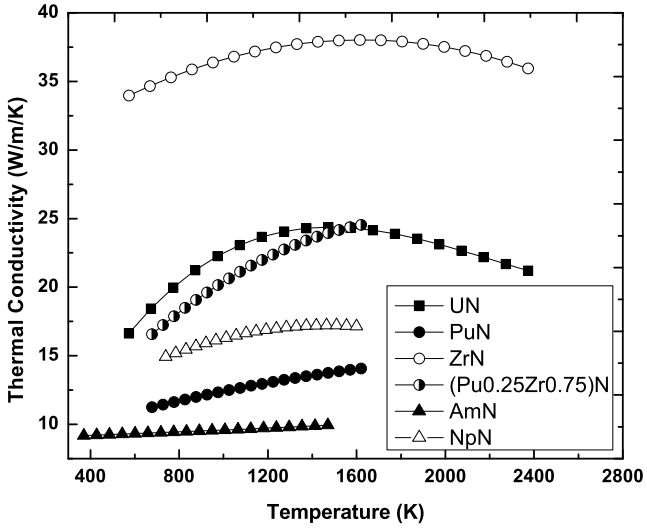


**Figure 5.11.** Thermal conductivity of actinide nitrides

$$\begin{aligned} k(Np,Pu,Am,Zr)N &= c(Np)k(NpN) + c(Pu)k(PuN) \\ &+ c(Am)k(AmN) + c(Zr)k(ZrN) \end{aligned} \tag{5.5}$$

In order to estimate the burn up effect on thermal conductivity of nitride fuel, mainly incurred by porosity build up, the Maxwell-Eucken correction was applied as expressed in Eq. 5.6 [89], in which P is porosity and $\beta$ equals 2.00 for (Pu,Zr)N [88]. Irradiation swelling rate of UN can be calculated based on Eq. 5.7, in which $T_{fuel,ave}$, Bu and $\rho$ stand for the average fuel temperature (in Kelvin), the fuel burnup (in at.%) and the as-fabricated fuel density (in % theoritical density, TD) respectively [90]. The irradiation swelling of nitride fuel is assumed to be caused only by the porosity build-up. These correlations are proved to be valid for (U,Pu)N based on in-pile data obtained from irradiation tests in JOYO reactor [91]. Hence, they are also assumed to be valid for nitride composite and nitride fuels discussed in Paper **II** and **IV**.

$$k = k_0 \frac{1-P}{1+P\beta} \tag{5.6}$$

$$\Delta V/V(\%) = 4.7 \times 10^{-11} T_{fuel,ave}^{3.12} Bu^{0.83} \rho^{0.5} \tag{5.7}$$

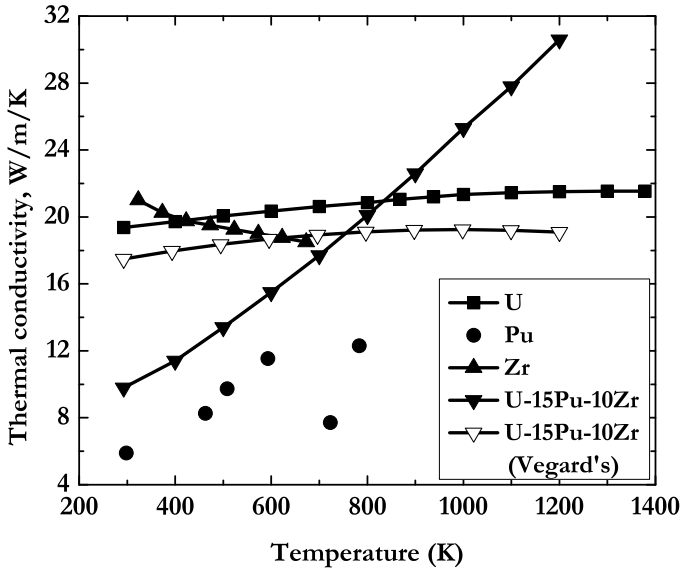


**Figure 5.12.** Thermal conductivity of actinide metals and alloys

### Metallic fuel, Ac+Zr alloy

Since thermal conductivities of metallic fuels discussed in Paper **III** are currently not available in open literature, a proper assumption should be raised to estimate the thermal conductivity of Ac+Zr alloys with various concentrations of americium. As can be noticed from Fig. 5.12, if the Vegard's law was applied, the calculated thermal conductivity of U-Pu-Zr alloy based on thermal conductivities of different actinide metals [92] will be lower than the one reported for U-15Pu-10Zr loaded into EBR-II in the temperature region of 800-1000 K, which is the working temperature region of metallic fuel in IFR during normal operating conditions. Hence, being a conservative assumption, the Vegard's law was used to calculate thermal conductivities of metallic fuel alloys.

The impact from the irradiation on the thermal conductivity of metallic fuel is mainly due to the porosity construction and fission products generation. The volumetric swelling rate of metallic alloy fuels was reported to be 30% for 2.0 at.% burnup and then stablize at this level at least up to 15 at.% burnup [94], which is the burnup level when the EOC state of IFR was reached. If we assume the bulk swelling of metallic fuels is only caused by open porosity construction, the porosity needed for 30% volumetric swelling is around 25%. Since metallic fuel colume is bonded by liquid sodium, which has much higher thermal conductivity than actinide metals and will fill the open porosity in metallic fuel, the impact from porosity construction

can be neglected. However, thermal conductivity of metallic fuel alloy experienced more than 2 at.% burnup was still reported to have a reduction of approximately 20%, which is due to the accumulation of fission products [97].

### 5.2.2 Fuel melting point

#### Oxide fuel

For simulations performed in Paper **I**, fuel failure starts when solidus temperature of fuel was offset. Solidus and liquidus temperatures of oxide fuel can be calculated by applying Vegard's law [95] as:

$$\begin{aligned} T_{sol} &= T_{UO_2}c_U + T_{PuO_2}c_{Pu} + T_{AmO_2}c_{Am} + C_{sol} \\ T_{liq} &= T_{UO_2}c_U + T_{PuO_2}c_{Pu} + T_{AmO_2}c_{Am} + C_{liq} \end{aligned} \tag{5.8}$$

in which c stands for atomic fractions of different elements. $T_{UO_2}$, $T_{PuO_2}$ and $T_{AmO_2}$ stand for melting points of $UO_2$, $PuO_2$ and $AmO_2$, equalling 3120 K, 2663 K and 2783 K respectively [96]. $C_{sol}$ and $C_{liq}$ are the corrections for solidus and liquidus temperatures, which can be obtained with:

$$\begin{aligned} C_{sol} &= -121c_U c_{Pu} - 340b - 1000|x| \\ C_{liq} &= 129c_U c_{Pu} - 340b - 300|x| \end{aligned} \tag{5.9}$$

in which $c_U$, $c_{Pu}$, b, |x| stand for atomic fraction of U, atomic fraction of Pu, fuel burnup, absolute value of the stoichiometric deviation respectively.

#### Inert matrix nitride for ADS

Since dissociation temperatures of UN, PuN, NpN and AmN are much lower than their corresponding congruent melting temperatures if partial pressure of nitrogen is less than 0.15 MPa, failure point of (Pu,Am,Zr)N is assumed to be the temperature when 0.01% AmN dissociates into metallic Am and nitrogen gas, concerning the relocation of Am in liquid phase. Based on the calculation results from the Thermo-Calc code applying ALCHYMY database, the failure point of $(Pu_{0.2}Am_{0.3}Zr_{0.5})N$ compound in a small volume, such as an intact fuel cladding, is equal to 2400 K [93]. Burn up effects on the failure point of nitride fuel was neglected.

#### Nitride fuel for SFR

The dissociation temperature of (U,Pu,Am)N was also calculated by the Thermo-Calc code based on design details of BN1200 fuel pins as listed in Table 5.2. If the decomposition tolerance of AmN was set at 0.01 at.%, the estimated working limit of nitride fuel containing 9.0 wt.% Am is 2400 K.

#### Metallic fuel alloy

Solidus temperature of Pu-40Zr alloy was reported as 1507 K, which was assumed to be valid for the solidus temperatures of other Pu-Am-Np-Zr alloys before any exper-

**Table 5.2.** Design details needed for decomposition simulations of nitride fuels

| Parameter | Value | Parameter | Value |
|---|---|---|---|
| Fuel column | | | |
| Density, g/cm$^3$ | 12.9 | Radius, mm | 3.81 mm |
| Length, mm | 850 | Mass, kg | 0.50 |
| Fuel pin | | | |
| Gas plenum length, mm | 400 | Cladding inner radius, mm | 4.00 |
| Gas plenum volume, m$^3$ | $2.01\times10^{-5}$ | Pin tube volume, m$^3$ | $6.28\times10^{-5}$ |
| Fission gases, 9 wt.% Am, 114 MWd/kgHM burnup, 623 K | | | |
| Gaseous elements | He, Kr, I, Xe | Gas release rate, % | 20 |
| Fission gas amount, mol | 0.26 | Gas pressure, MPa | 14.0 |

imental data was obtained [94]. However, since solidus temperatures of U-included fuels, e.g., U-20Pu-10Zr and U-19Pu-10Zr, was reported to be lower than this value, the author decided to use the solidus temperature of U-19Pu-10Zr, equalling 1350 K, as the solidus temperature of the metallic fuel alloy U-12Pu-10Zr with various Am contents.

As fission products generated during fuel burnup, rare earth (RE) elements, e.g., La, Ce and Y, may lead to the decrease of the melting point of the compound formed by Fuel Cladding Chemical Interactions (FCCI) between U-Pu-Am-Zr fuel alloy and Fe in stainless steel cladding. However, this phenomena was reported to happen only when RE concentration is higher than 5% [98]. Fortunately, the concentration of RE is only ∼3% after 140 MWd/kgHM burnup was achieved. Thus, no severe impact will be expected from burnup on melting characteristics of U-Pu-Am-Zr alloys.

### 5.2.3 Heat capacity

Since differences between heat capacities of different actinide oxides are negligibly small up to 2500 K as shown in Fig. 5.13, heat capacities of the MOX fuel modified by different fractions of Am for BN600 usage was simply assumed to be equal to the heat capacity of MOX fuel containing 25 at.%. Due to the small mass of fuel material loaded into each fuel pin, the discrepancy incurred by this assumption could be limited at a low level during transient simulations.

$$\begin{aligned} Cp_(U,Pu,Am,Zr)N &= x_U \times Cp_UN + x_Pu \times Cp_PuN \\ &+ x_Am \times Cp_AmN + x_Zr \times Cp_ZrN \end{aligned} \tag{5.10}$$

Heat capacities of (U,Pu,Am,Zr)N, being loaded into the suggested ADS design, was recommended to be calculated based on the Kopp-Neumann law [88] as expressed in Eq. 5.10, in which x stands for molecular fraction of different metallic

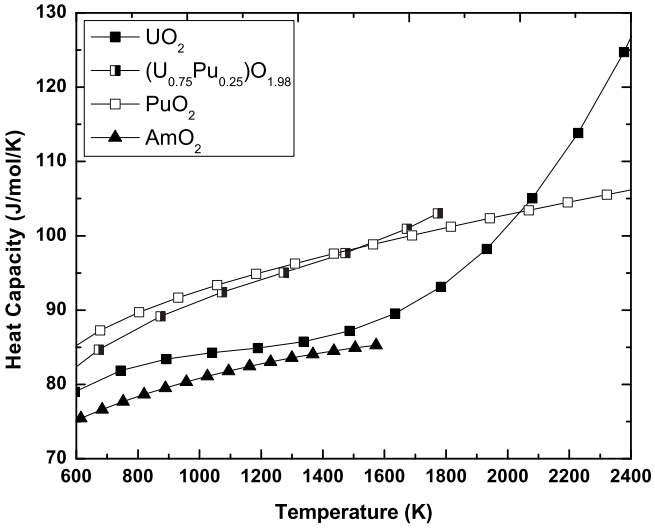


**Figure 5.13.** Heat capacities of actinide oxides, [80], [99], [100]

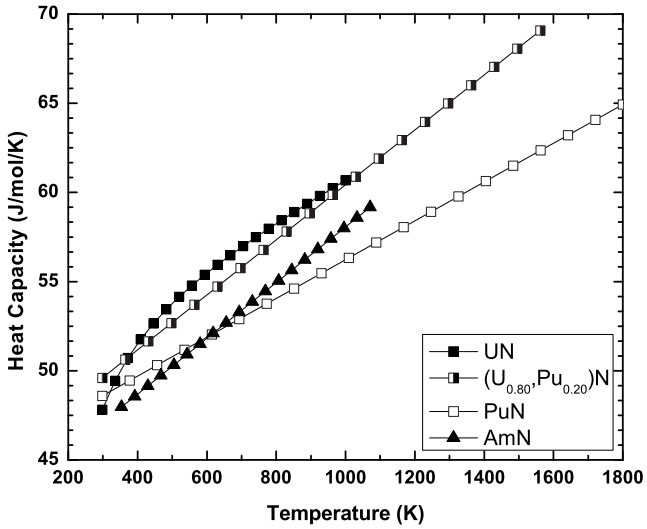


**Figure 5.14.** Heat capacities of AcN and (Ac,Zr)N, [101], [102], [79]

**Table 5.3.** Heat capacities of actinide metals

| Element | Correlation, J/mol/K | Valid temperature, K |
|---|---|---|
| U [92] | $5.37 \times 10^{-3}$ T + $10.18 \times 10^{-5}$T$^2$ | 293-942 |
| Pu,$\alpha$-$\delta$ [92] | 32$\sim$37 | 298-783 |
| Am,$\alpha$ [104] | 30.04-29.05 $\times$ 10 $^{-3}$ T + 52.03 $\times$ $10^{-6}$ T$^2$ - 18.96 $\times$ $10^{-9}$ T$^3$ | 293-1042 |
| Zr [105] | 26.66+1.37 $\times 10^{-2}$ | 423 - 1273 |

elements. $Cp_{UN}$, $Cp_{PuN}$, $Cp_{AmN}$ and $Cp_{ZrN}$ are heat capacities of UN, PuN, AmN and ZrN calculated by correlations shown in Fig. 5.14. Heat capacity of actinide nitride fuels loaded into the BN1200 reactor could also calculated based on Eq. 5.10.

The Kopp-Neumann law was also reported to be valid for metallic fuel alloys [94]. Heat capacities of U-Pu-Am-Zr alloys discussed in Paper **III** for IFR usage could then be calculated from individual heat capacities of U, Pu, Am and Zr, which are obtained or third order extrapolated from correlations listed in Table 5.3.

Due to limited information available in open literature, the burnup effects on heat capacities of oxide, nitride and metallic fuels were neglected in this thesis' study.

# Chapter 6

# Results and discussions

## 6.1 Transient simulation results

In Paper **I**, **III** and **IV**, transient analysis was performed for MOX fuel loaded BN600 reactor, metallic fuel loaded IFR and nitride fuel loaded BN1200. In order to parameterize the impact from Am introduction on core safety behavior, different fractions of Am has been introduced into the oxide, metallic and nitride fuels, maintaining the Pu content.

Core safety behavior of the nitride fuel loaded ADS design proposed in Paper **II**, with respect to postulated transients, has also been investigated.

Coolant boiling, thermal creep rupture of cladding and fuel melting (or decomposition of actinide nitrides) were considered as design limits to terminate transient simulations.

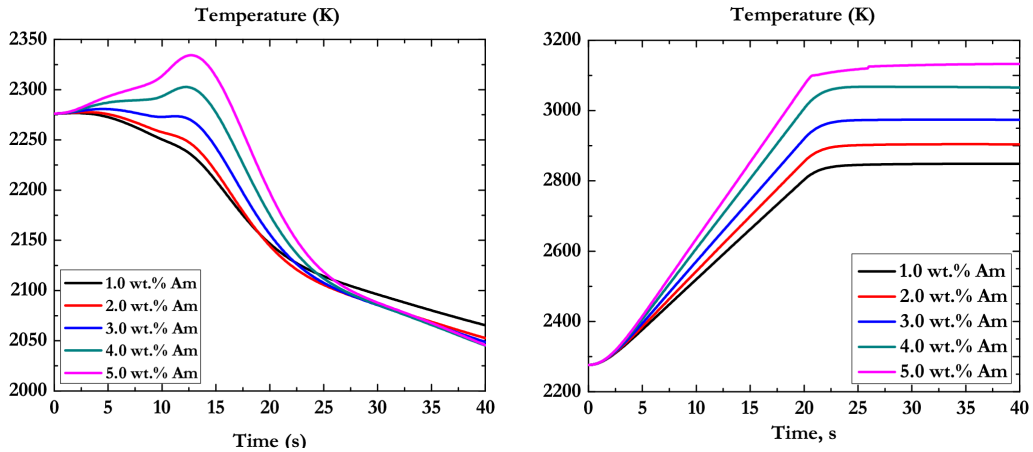


**Figure 6.1.** The maximum fuel temperature for oxide core during ULOF (left) and UTOP (right) transients, $P_{max}$=37 kW/m

As shown in Fig. 6.1, 6.2 and 6.3, during UTOP transient, fuel temperatures

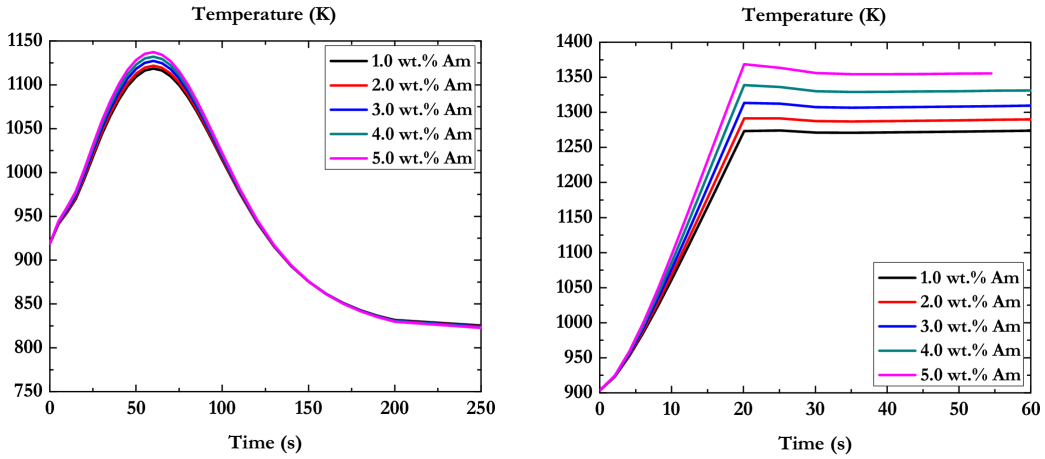


**Figure 6.2.** The maximum fuel temperature for metal core cladded with HT9 stainless steel during ULOF (left) and UTOP (right) at BOC, $P_{max}$=33 kW/m

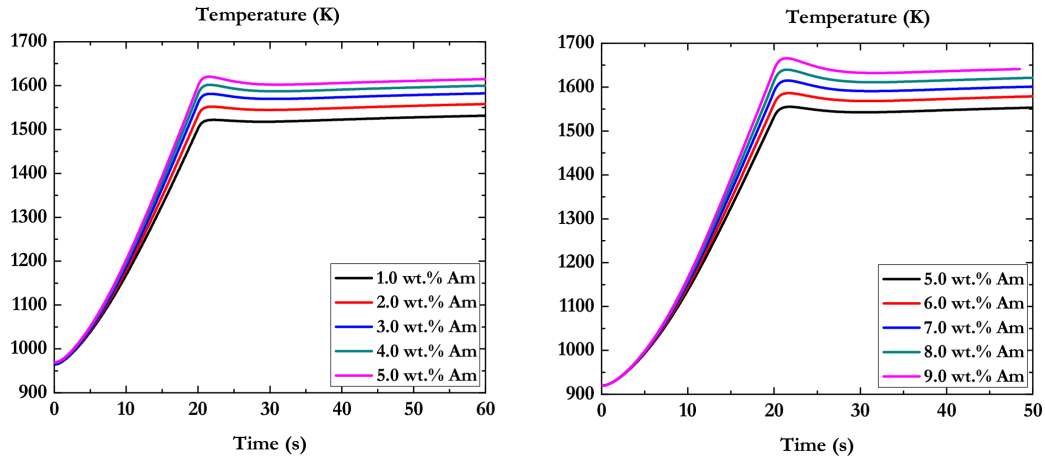


**Figure 6.3.** The maximum fuel temperature for nitride core during UTOP transient at EOEC, with $P_{max}$=37 kW/m (left) and $P_{max}$=33 kW/m (right)

at fuel column hot spot will increase with Am concentration, which is mainly due to the degradation effect from Am introduction on the Doppler effect of fuels as can be noticed from Fig. 5.3. For cases with 1.0 wt.% $\sim$ 5.0 wt.% Am contents in oxide, metallic and nitride fuels loaded into BN600, IFR and BN1200 (with $P_{max}$=37 kW/m) cores respectively, the maximum fuel temperatures was reported to increase by around 300 K, 100 K and 170 K, leading to 6%, 3% and 3% power penalties per percent additional Am introduction if sufficient margin to fuel failure needs to be maintained. During ULOF transient, maximum fuel temperatures are well below working limits of oxide, metallic and nitride fuels, thanks to the strong negative

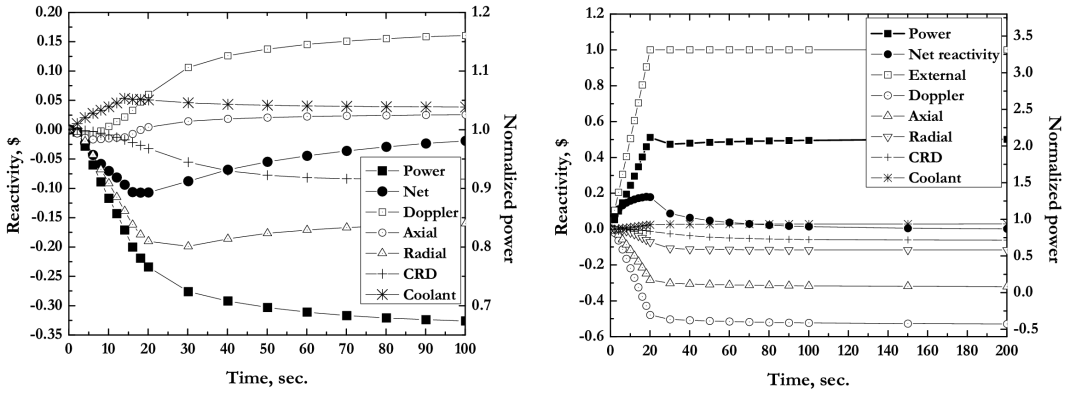


**Figure 6.4.** Power and reactivity feedbacks of oxide core with 1.0 wt.% Am at BOC during ULOF (left) and UTOP (right) transients, $P_{max}$=37 kW/m

reactivity responses from radial thermal expansion of fuel assembly diagrids, which will stablize core power at a relatively low level as can be noticed from Fig. 6.4.

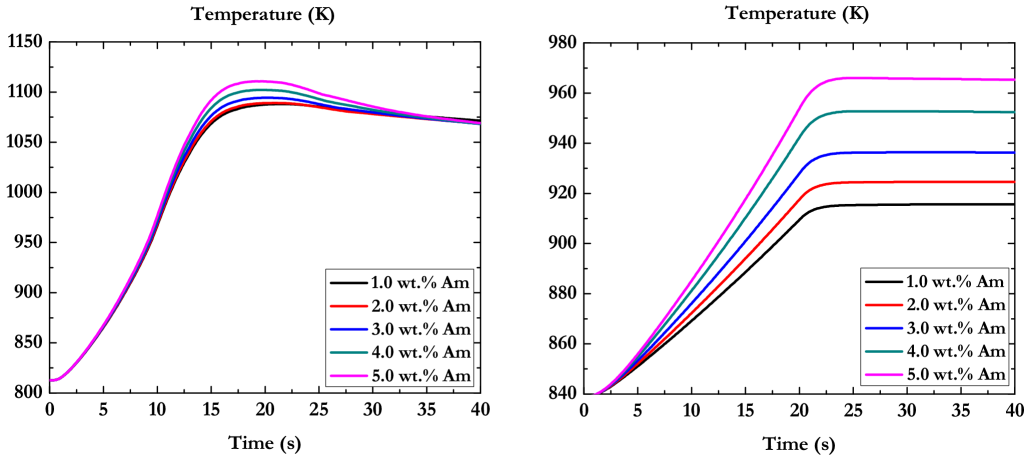


**Figure 6.5.** Cladding inner surface temperature for oxide core during ULOF (left) and UTOP (right) transients, $P_{max}$=37 kW/m

It can be noticed from Fig. 6.5, 6.6 and 6.7 that: the highest cladding temperatures that can be reached during ULOF and UTOP transients at the reference power rating determined above, are 70 K, 300 K and 400 K lower than the predetermined creep rupture limits of cladding materials for oxide, metal and nitride cores usage.

The boiling point of liquid Na coolant was determined by the static pressure on the coolant inventory. For all cases investigated in Paper **I**, **III** and **IV**, coolant

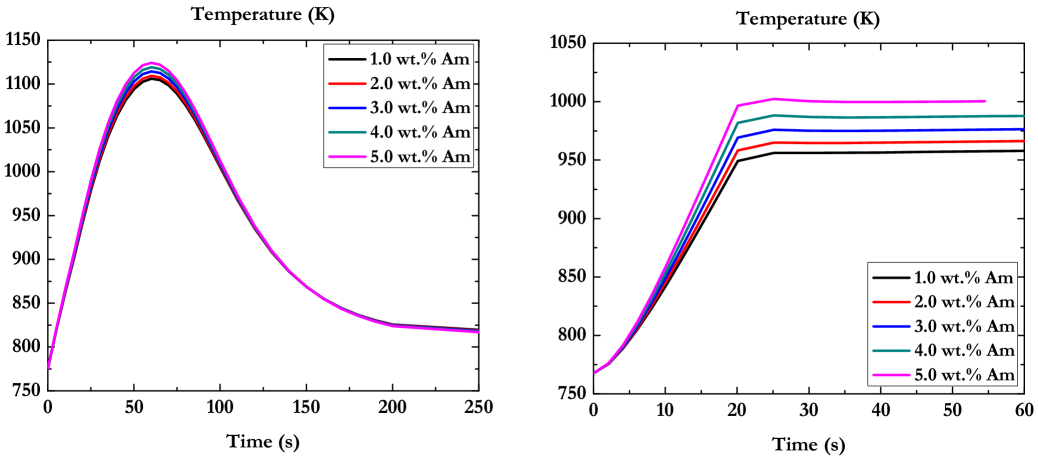


**Figure 6.6.** Cladding inner surface temperature for metal core cladded with HT9 stainless steel during ULOF (left) and UTOP (right) transients at BOC, $P_{max}$=33 kW/m

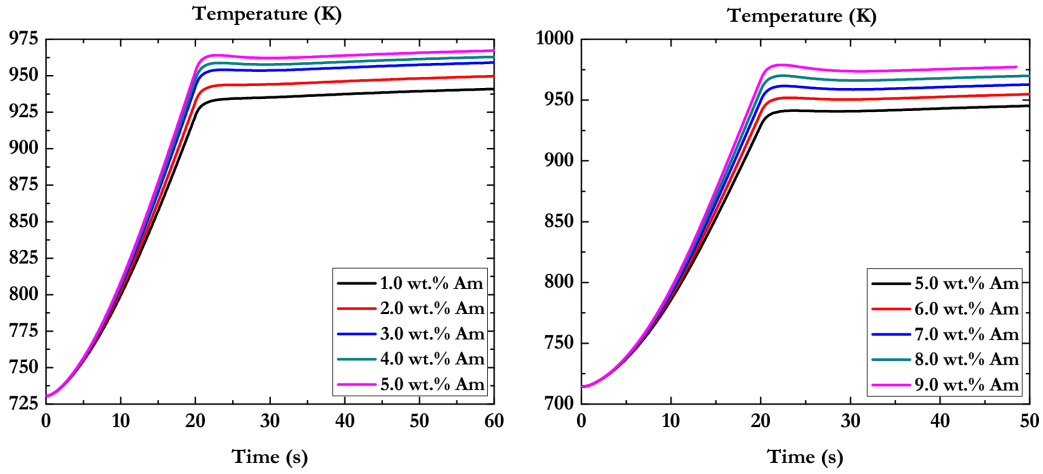


**Figure 6.7.** Cladding inner surface temperature for nitride core during UTOP transient at EOEC, with $P_{max}$=37 kW/m (left) and $P_{max}$=33 kW/m (right)

boiling was not reported by the SAS4A/SASSYS code, thanks to negative reactivity responses from structure radial expansion, the Doppler effect and fuel pin axial expansion as shown in Fig. 6.4.

Core performances, with respect to Unprotected Loss-of-Offsite-Power (ULOOP) transient, were also investigated in Paper **III** and **IV** for metallic fuel loaded IFR and nitride fuel loaded BN1200. Although the cladding rupture time calculated based on 30 minutes surviving time was offset around 50 seconds into the transient,

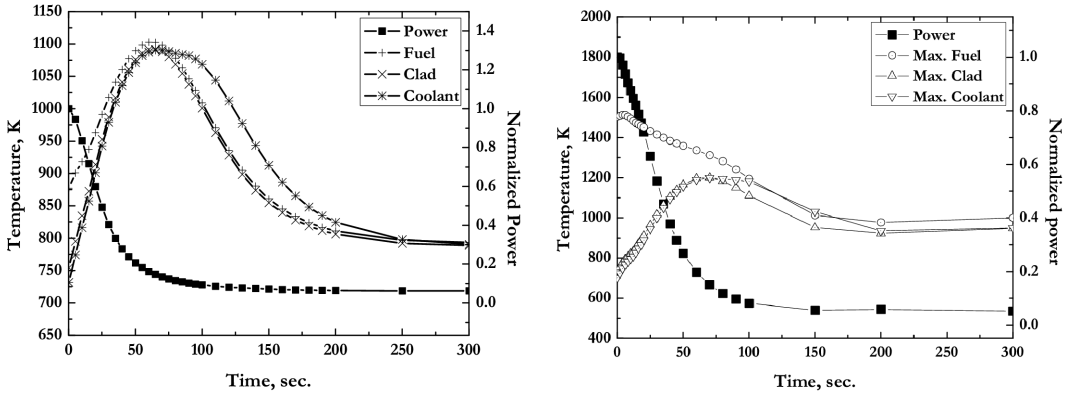


**Figure 6.8.** Power and temperatures of metal core (right) with $P_{max}$=33 kW/m and nitride core (left) with $P_{max}$=37 kW/m with 1.0 wt.% Am during ULOOP at BOC

the time period for the cladding temperature staying above the rupture limit was reported to be less than 50 seconds, then the core power will be dragged down to the decay power level by the strong negative reactivity response incurred by structure radial expansion as shown in Fig. 6.8, leading to the reduction of fuel, cladding and coolant temperatures. Hence, cladding creep rupture was considered not to occur during ULOOP transients.

In Paper **II**, safety analysis of the suggested ADS design with 1.20 cm pin pitch was performed. Maximum fuel and coolant temperatures that were reached during the postulated transients are 1727 K and 1122 K, preserving around 700 K margin to fuel failure and 900 K margin to coolant boiling respectively as shown in Table 6.1. The cladding's asymptotic temperature during transients is limited to less than 1070 K, preserving more than 130 K margin to pin cladding burst. Thus, this ADS design could be confirmed to survive the full transients.

The cladding hot spot temperature during normal operating condition is equal to 789 K, preserving approximately 40 K margin to rupture limit in terms of thermal creep, irradiation damage and HLM corrosion.

The reactor vessel's asymptotic temperature during transients is limited to less than 690 K, which is approximately 30 K lower than the reported creep limit of the reactor vessel, under which the reactor vessel integrity can be assured [106].

## 6.2 Am transmutation efficiencies

Thanks to the build-in sub-criticality, safety behavior of ADS in case of a rapid external reactivity insertion is much better than those of critical systems, in which a prompt super-criticality may easily be ignited. Hence, higher Am concentration, leading to significant degradations on core safety parameters, could be permitted

**Table 6.1.** Transient simulation results for the suggested ADS design

| Transient | ULOF | UTOP | PLOHS |
|---|---|---|---|
| BOC | | | |
| $T_{fuel}^{max}$ [K] | 1727 | 1507 | 1109 |
| $T_{clad}^{max}$ [K] | 1145 | 900 | 851 |
| $T_{clad}^{final}$ [K] | 1068 | 900 | 823 |
| $T_{LBE}^{max}$ [K] | 1118 | 859 | 850 |
| Normalized $P_{final}$ | 0.97 | 1.42 | 0.06 |
| $\Delta\rho_{net}^{max}$ [\$] | -0.83 | 6.29 | 0.75 |
| Normalized $\dot{m}_{final}$ | 0.44 | 1.02 | 0.09 |
| EOC | | | |
| $T_{fuel}^{max}$ [K] | 1497 | 1121 | 864 |
| $T_{clad}^{max}$ [K] | 1149 | 898 | 856 |
| $T_{clad}^{final}$ [K] | 1069 | 898 | 823 |
| $T_{LBE}^{max}$ [K] | 1122 | 857 | 856 |
| Normalized $P_{final}$ | 0.98 | 1.41 | 0.06 |
| $\Delta\rho_{net}^{max}$ [\$] | -0.75 | 6.00 | 1.02 |
| Normalized $\dot{m}_{final}$ | 0.44 | 1.02 | 0.09 |

for homogeneous loading into ADS. Besides, spallation neutrons produced by accelerated proton beam through (p,n) reactions have higher average energy than the ones from fission or decay reactions, which leads to a higher energy of the averaged neutron flux in ADS than the one in critical reactors. Thus, the Am transmutation rate in the present ADS design loaded with nitride composite fuel, having improved neutron economy than the reference EIFT-400 core, was designed to be 43 kg/$TWh_{th}$, which is more than ten times higher than the ones achieved by SFRs loaded with oxide, metallic and nitride fuels for their reference case with 1.0 wt.% Am content.

However, as can be noticed from Fig. 6.9, Am transmutation rate varies for different fuel types and increases with Am content's increasing. It means that a comparable Am burning rate, with respect to the one achieved by the present ADS, may be achieved in a sodium cooled critical fast reactor, if we could properly choose the fuel type and also the Am content in the fuel.

Since metallic fuel has a higher atomic fraction of heavy metal (Ac:Zr $\approx$ 3:1) than the oxide fuel (Ac:O = 1:2) and Zr atoms in metallic fuel matrix has smaller moderation effect than nitrogen atoms in nitride fuel matrix, the highest Am burning rate can be provided by the metallic fuel loaded IFR core for the same Am concentration. Thanks to the same atomic fraction of heavy metal in the nitride fuel (Ac:N = 1:1) as the one in the metallic fuel, the nitride fuel loaded BN1200 can provide slightly lower Am burning rates than the metallic fuel loaded IFR. Besides, BN1200 can work at a higher power rating than IFR because of the higher work-

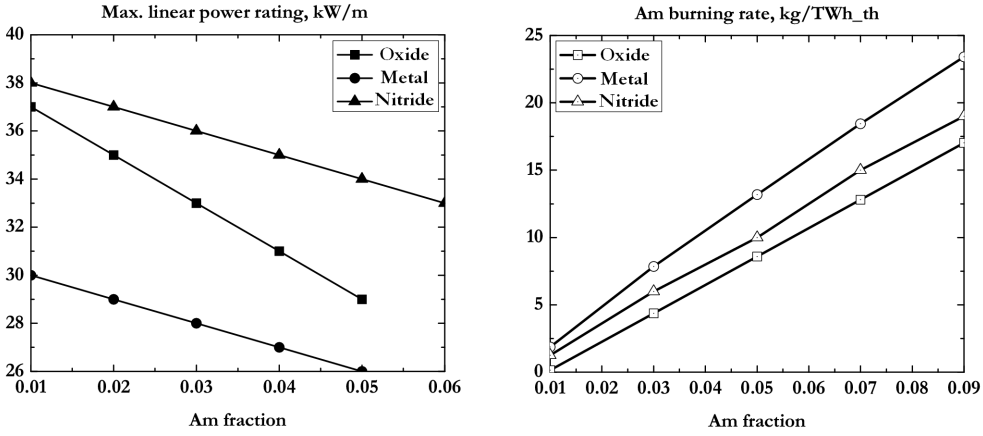


**Figure 6.9.** Maximum permitted linear power rating (left) and Am transmutation rate (right) for different Am contents and reactor designs

ing limit of nitride fuel comparing to that of metallic fuel. Hence, among all SFR designs discussed in this thesis loaded with three different types of fuel, the highest Am transmutation efficiency can be expected from the nitride fuelled core.

For the suggested ADS having 43 kg/TWh$_{th}$ consumption rate of Am and 201 MW$_{th}$ power rating, the capital cost per unit power rating will increase by approximately 40% due to the implementation of the proton beam [107]. If a 30% power penalty, leading to the same cost penalty, was allowed the SFRs investigated in this thesis, the introduction of 8 wt.% Am into nitride fuel for the BN1200 reactor usage can be permitted as extropolated from Fig. 6.9. At this Am content, a 16 kg/TWh$_{th}$ Am burning rate can be provided by the nitride fuel loaded BN1200 reactor. For the metallic fuel loaded IFR, 7 wt.% Am content, providing a 17 kg/TWh$_{th}$ Am burning rate, can be permitted, if 30% power penalty was accepted.

Since the Am generation rate of one 1000 MWe (3400 MW$_{th}$) grade LWR was reported to be 0.55 kg/TWh$_{th}$ after 60 MWd/kgHM burnup and 10-year cooling [108], **one** BN1200 type SFR operating with 70% of its reference power rating (2900 MW$_{th}$) can provide an Am burning rate of 16 kg/TWh$_{th}$ and is then sufficient to transmute the Am inventory generated by **16** commercial LWRs with 1000 MWe power rating in the same time period. The metallic fuel loaded IFR operating with 70% of its reference power rating (2500 MW$_{th}$) can provide 17 kg/TWh$_{th}$ Am burning rate, the supporting ratio will then be slightly lower, being equal to one IFR per 15 1000 MWe grade LWRs. In comparison, **one nitride fuelled ADS** in the suggested design is only sufficient to transmute the Am inventory generated by **five** 1000 MWe grade LWRs in the same time period. Thus, one SFR could provide a higher transmutation capability than one ADS operating at 7 times lower power rating. However, the fraction of ADS power in power park (≈0.015), calculated by $P_{ADS}/(P_{ADS} + 5\times P_{LWR})$, is still lower than that of the most efficient SFR

($\approx$0.037), calculated by $\mathrm{P}_{SFR}/(\mathrm{P}_{SFR} + 16\times\mathrm{P}_{LWR})$.

# Chapter 7

# Conclusions

The upper limit to the amount of Am that can be loaded into a medium sized sodium cooled fast reactor was once reported as 2-3%. However, after performing transient analysis with the SAS4A/SASSYS code for SFRs loaded with oxide, metallic and nitride fuels, no solid limit was observed. Instead, higher Am contents, aiming at higher Am transmutation rates, can be permitted, if specific power penalties were allowed.

Based on results obtained from the SAS4A/SASSYS transient simulations, the suggested ADS design with 1.20 cm pin pitch, providing a MA transmutation rate of 42 kg/TWh$_{\text{th}}$, could survive the full set of transients, thanks to switching the cladding material from the reference T91 stainless steel to the austenitic 15/15Ti stainless steel with higher thermal creep strength.

One nitride fuelled ADS with the power rating of 201 MW$_{\text{th}}$ and the consumption rate of Am equalling 43 kg/TWh$_{\text{th}}$ is sufficient to transmute the Am inventory generated by five 1000 MWe grade LWRs within the same operating time. In comparison with the suggested ADS design with 40% cost penalty incurred by the implementation of accelerated proton beam, supporting ratios reported for the metallic fuel loaded IFR and nitride fuel loaded BN1200 are significantly improved to one IFR with the power rating of 1750 MW$_{\text{th}}$ per 15 LWRs and one BN1200 with the power rating of 2050 MW$_{\text{th}}$ per 16 LWRs respectively. The total fraction of ADS power in the power park, however, is only half of the case for critical reactors, with corresponding smaller need for manufacture of americium bearing fuels.

# Bibliography


[1] IAEA, *Country Waste Profile Report for Hungary*, 2005.

[2] U.S. Nuclear Regulatory Commission, *Radioactive Waste: Production, Storage, Disposal*, **NUREG/BR-0216**, 2002.

[3] S. Esbjöm, *The cost of the Swedish nuclear waste program*, Progress in nuclear energy, **48**(4): 314-324, 2006.

[4] V. M. Efremenkov, *Radioactive waste management at nuclear power plants, An overview of the types of low- and intermediate-level wastes and how they are handled*, IAEA-1989/4, pp.37-42, 1989.

[5] D. G. Foster et al., *Review of PNL Study on Transmutation Processing of High Level Waste*, LA-UR-74-74, Los Alamos Scientific Laboratory, 1974.

[6] Jean-Pierre Revol, *An accelerator-driven system for the destruction of nuclear waste*, Progress in Nuclear Energy, **38**(1-2): 153-166, 2001.

[7] K. Kawashima, K. Kobayashi, K. Kaneto, *Utilization of fast reactor excess neutrons for burning long lived fission products*, Progress in Nuclear Energy, **29**(1): 281-288, 1995.

[8] Hüseyin Yapici, Gamze Genc, Nesrin Demir, *A comprehensive study on neutronics of a lead-bismuth eutectic cooled accelerator-driven sub-critical system for long-lived fission product transmutation*, Annals of Nuclear Energy, **35**(7): 1264-1273, 2008.

[9] K. Abrahams, *Safety and environmental aspects of partitioning and transmutation of actinides and fission products*. Proceedings of a technical committee meeting, International Atomic Energy Agency, IAEA-TECDOC-783, pp:149-159, 1993.

[10] Institut für Energieforschung (IEF), Forschungszentrum Jülich GmbH, *RED-IMPACT: Impact of Partitioning, Transmutation and Waste Reduction Technologies on the final Nuclear Waste Disposal*, ISSN 1866-1793, ISBN 978-3-89336-538-8, pp. 115-116, 2007.

[11] Daniel Westlén, *Reducing radiotoxicity in the long run*, Progress in Nuclear Energy, **49**(8):597-605, 2007.

[12] N. E. Holden, *Total and spontaneous fission half-lives for americium and curium nuclides half-lives for uranium, plutonium*, Pure & App, Chem., Vol. 61, No. 8, Brookhaven National Laboratory, USA, pp.1483-1504, 1989.

[13] Janne Wallenius, *Transmutation of nuclear waste*, Chapter 1, pp. 11, 2011.

[14] I. C. Gauld and B. D. Murphy, *Technical basis for a proposed expansion of regulatory guide 3.54-decay heat generation in an independent spent fuel storage installation*, NUREG/CR-6999, ORNL/TM-2007/231, Oak Ridge National Laboratory (ORNL), 2010.

[15] M. Delpech et al., *The Am and Cm transmutation, physics and feasibility*, In International Conference on Future nuclear systems, GLOBAL 99, 1999.

[16] P. E. Spivak, et al., *Measurements of $\eta$, for U233, U235 and Pu239 with Neutrons in the Energy Range 30 to 900 keV*, Journal Nuclear Energy, **4**:79-85, 1957.

[17] M. Salvatores, *Transmutation: Issues, Innovative options and Perspectives*, Progress in Nuclear Energy, **40**(3-4):375-402, 2002.

[18] http://www.euronuclear.org/1-information/generation-IV.htm

[19] Mamoru Konomur and Masakazu Ichimiya, *Design Challenges for Sodium Cooled Fast reactors*, Journal of Nuclear Materials, **371**(1-3):250-269, 2007.

[20] Nuclear Power Technology Development Section (IAEA), *Fast Reactor Database*, IAEA-TECDOC-866, pp.22-26, 1996.

[21] E. E. Shpil'rain, et al., *Density and Thermal Expansion of Liquid Alkali Metals, in Handbook of Thermodynamic and Transport Properties of Alkali Metals*, Blackwell Science Publications, Boston, 1985.

[22] L.H. Martin and K. C. Lang, *The thermal conductivity of water*, Proceedings of the Physical Society, **45**(4): 523-529.

[23] K. Buksha et al., *Operation experience of the BN-600 fast reactor*, Nuclear Engineering and Design, **173**(1-3): 67-79, 1997.

[24] V. Cherny et al., *Research Co-ordination Meeting on "Updated Codes and Methods to Reduce the Calculational Uncertainties of Liquid Metal Fast Reactor Reactivity Effects*", IAEA-RC-803.2, TWG-FR/103, Vienna, Austria, pp. 304-337, 2000.

[25] A. Danilytchev et al., *Reactivity Coefficients in Test Model IAEA (Phase 4)*, IAEA-RC-803.4, TWG-FR/113, Obninsk, Russia, pp. 245-271, 2003.

[26] S. I. Porollo et al., *Swelling and microstructure of austenitic stainless steel ChS-68 CW after high dose neutron irradiation*, Journal of Nuclear Materials, **393**(1): 61-66, 2009.

[27] Alan E. Waltar and Albert B. Reynolds, *Fast Breeder Reactors*, Pergamon Press, pp. 776-779, 1981.

[28] U.S. Department of Energy, Grand Junction Office, *Statistical data of the uranium industry*, GJO-100(82), 1983.

[29] TRADETECH, *The source for uranium price and industrial news since 1968*, http://www.uranium.info/

[30] Kiyoto Aizawa, *Consideration on safety research strategy toward commercialization of FBRs*, Progress in Nuclear Energy, **32**(3-4):255-262, 1998.

[31] J. K. Fink, *Results of Cursory Literature Review on Lead Thermophysical Properties*, ANL Intra-Laboratory Memo, 1998.

[32] W. Maschek et al., *Safety and design concepts of the 400 MWth-class EFIT accelerator driven transmuter and considerations for further developments*, Energy Conversion and Management, **51**(9): 1764-1773, 2010.

[33] Youpeng Zhang and Janne Wallenius, *Transmutation of americium in a medium size sodium cooled fast reactor design*, Annals of Nuclear Energy, **37**(5): 629-638, 2010.

[34] B. F. Gromov, Y. I. Orlov, P. N. Martynov, V. A. Gulevskiy, *The problems of technology of the heavy liquid metal coolants (lead-bismuth, lead)*, Proceedings of the Conference of the Heavy Liquid Metal Coolants in Nuclear Technology, Obninsk, Russian Federation, pp.87-100, 1998.

[35] S. Z. Verhovodko and V. V. Zamukov, *The experience of designing, using and utilizing the nuclear power installations with lead-bismuth liquid metal coolant for the "Alpha" type nuclear submarines*, Proceedings of the conference "Heavy liquid metal coolants in nuclear technology", pp. 18-23, 1998.

[36] H. U. Wider, J. Carsson and E. Loewen, *Renewed Interest in Lead Cooled Fast Reactors*, Progress in Nuclear Energy, **47**(1-4):44-52, 2005.

[37] Giacomino Bandini, Paride Meloni and Massimiliano Polidori, *Thermal-hydraulics analyses of ELSY lead fast reactor with open square core option*, Nuclear Engineering and Design, **241**(4):1165-1171, 2011.

[38] Allen L. Johnson et al., *Spectroscopic and microscopic investigation of the corrosion of 316/316L stainless steel by leadŰbismuth eutectic (LBE) at elevated temperatures: importance of surface preparation*, Journal of Nuclear Materials, **328**(2-3):88-96, 2004.

[39] Nuclear Energy Angency (NEA), *Handbook on lead-bismuth eutectic alloy and lead properties, materials compatibility, thermal-hydraulics and technologies*, Chapter 4, pp. 130-135, 2007.

[40] Jinsuo Zhang, *A review of steel corrosion by liquid lead and lead-bismuth*, Corrosion Science, **51**(6):1207-1227, 2009.

[41] A. Ide, Y. Takenakat and S. Maeda, *A study on utilization of heat of high temperature gas-cooled reactors*, Progress in Nuclear Energy, **29**:201-208, 1995.

[42] T. D. Newton and P. J. Smith, *Flexibility of the Gas Cooled Fast Reactor to Meet the Requirements of the 21$^{st}$ Century*, Gen-IV International Forum (GIF).

[43] P. Anzieu, R. Stainsby and K. Mikityuk, *Gas-cooled fast reactor (GFR): overview and perspectives*, GIF Symposium, Paris (France), 2009.

[44] Helge Petersen, Danish Atomic Energy Commission, *The properties of helium: density, specific heats, viscosity, and thermal conductivity at pressures from 1 to 100 bar and from room temperature to about 1800 K*, Chapter 1, pp. 6-7, 1970.

[45] G. Melese-d'Hospital and R.H. Simon, *Status of gas-cooled fast breeder reactor programs*, Nuclear Engineering and Design, **40**:5-12, 1977.

[46] M. Salvatores, and G. Palmiotti, *Radioactive waste partitioning and transmutation within advanced fuel cycles: achievements and challenges*, Progress in Particle and Nuclear Physics, **66**(1):144-166, 2011.

[47] J. Tommasi et al., *Long-lived waste transmutation in reactors*, Nuclear Technology, **111**:133-148, 1995.

[48] M. A. Smith, E. E. Morris and R. N. Hill, *Physics and safety studies of low conversion ratio sodium cooled fast reactors*, Proc. Int. Conf. GLOBAL 2003, New Orleans, 2003.

[49] C. Fazio et al., *Advanced nuclear fuel cycles and systems*, Proc. Int. Conf. Global 2007, Idaho, 2007.

[50] Kamil Tuček, Johan Carlssona and Hartmut Widera, *Nuclear Engineering and Design*, **236**(14-16):1589-1598, 2006.

[51] Alan Baxter and Carmelo Rodriguez, *The application of gas-cooled reactor technologies to the transmutation of nuclear waste*, Progress in Nuclear Energy, **38**(1-2):81-105, 2001.

[52] P. Seltborg, J. Wallenius, K. Tucek and W. Gudowski, *Definition and application of proton source efficiency in accelerator driven systems*, Nuclear Science and Engineering, **145**:390-399, 2003.

[53] A. V. Dementyev, N. M. Sobolevsky, Yu. Ya. Stavissky, *Neutron yield from extended lead target under incident protons of 0.1 to 100 GeV*, Nuclear Instruments and Methods in Physics Research A, **374**:70-72, 1996.

[54] J. Ales et al., *XX International Linac Conference*, BNL-6742.6, 2000.

[55] Nam-il Tak, Hans-Joachim Neitzel and Xu Cheng, *Computational fluid dynamics analysis of spallation target for experimental accelerator-driven transmutation system*, Nuclear Engineering and Design, **235**(7): 761-772, 2005.

[56] F. Sordo et al., *Material selection for spallation neutron source windows: Application to PDS-XADS and XT-ADS prototypes*, Nuclear Engineering and Design, **239**(11): 2573-2580, 2009.

[57] http://myrrha.sckcen.be/en/Engineering

[58] Andrei Fokau et al., *A source efficient ADS for minor actinides burning*, Annals of Nuclear Energy, **37**(4):540-545, 2010.

[59] R. Calabrese et al., *Heterogeneous fuels for minor actinides transmutation: Fuel performance codes predictions in the EFIT case study* , Annals of Nuclear Energy, **37**(6): 867-874, 2010.

[60] Jaakko Leppänen, *PSG2 / Serpent a Continuous-energy Monte Carlo Reactor Physics Burnup Calculation Code, Methodology-User's Manual-Validation Report*, 2008.

[61] Jaakko Leppänen, 2011, PSG2 / Serpent - a Continuous-energy Monte Carlo Reactor Physics Burnup Calculation Code, User's Manual, September 5, 2011

[62] Jaakko Leppänen, *Diffusion Code Group Constant Generation Using the Monte Carlo Method*, In Proc. XII Meeting on Reactor Physics in the Nordic Countries, Halden, 2005.

[63] J. E. Cahalan, SAS4A/SASSYS-1 Maintenance and Operations Handbook, Argonne National Laboratory, 2002.

[64] Nuclear Power Technology Development Section, *Transient and Accident Analysis of a BN-800 Type LMFR with near Zero Void Effect*, IAEA-TECDOC-1139, 2000.

[65] M. Eriksson, J. E. Cahalan and W. S. Yang, *On the Performance of Point Kinetics for the Analysis of Accelerator-Driven Systems*, Nuclear Science and Engineering, **149**(3): 298-311, 2005.

[66] O. M. Saraev, et al., Technical Committee Meeting, IAEA-TECDOC-907, Kalpakkam, 27-31, 1996.

[67] D.C. Wade, R.N. Hill, *The design rationale of the IFR*, Progress in Nuclear Energy, **31**(1):13-42, 1997.

[68] H. Tsai et al., "Review of Behavior of Mixed-Oxide Fuel Elements In Extended Over power Transient Tests in EBR-II", IL 60439-4838, Argonne National Laboratory, 1994.

[69] P. Hosemann, M. Hawley, G. Mori, N. Li, S.A. Maloy, *AFM and MFM characterization of oxide layers grown on stainless steels in lead bismuth eutectic*, Journal of Nuclear Materials, *376*(3):289-292, 2008.

[70] V. M. Poplavsky, et al., *Core design and fuel cycle of advanced fast reactor with sodium coolant*, International Conference on Fast Reactors and Related Fuel Cycles (FR09)-Challenges and Opportunities, Kyoto, Japan, 2009.

[71] M. Petrazzini, *EFIT fuel assembly pressure drop*, EUROTRANS Technical Report.

[72] W. Maschek et al., *Accelerator driven systems for transmutation: Fuel development, design and safety*, Progress in Nuclear Energy, **50**(2-6): 333-340, 2008.

[73] Kenneth Barbalace. Periodic Table of Elements. EnvironmentalChemistry.com, 1995-2010, http://EnvironmentalChemistry.com/yogi/periodic/Am.html

[74] David R. Lide, *89th Handbook of Chemistry and Physics*, Taylor&Francis Inc., 2008-2009.

[75] M. Salvatores et al., *Intercomparison of systems for TRU recycle at equilibrium*, Proc. Int. Conf. GLOBAL 2005.

[76] Pradyot Patnaik, *Handbook of Inorganic Chemicals*, McGraw-Hill Professional, 2003.

[77] P. del Marmol, *Delayed-neutron precursors*, Atomic Data and Nuclear Data Tables, **6**(2): 141-151, 1969.

[78] E. H. P. Cordfunke et al., *Thermochemical Data for Reactor Materials and Fission Products*, Elsevier, Amsterdam, 1990.

[79] Tsuyoshi Nishi et al., *Thermal conductivity of* $AmO_{2-x}$, Journal of Nuclear Materials, **373**(1-3):295-298, 2008.

[80] J. K. Fink, *Thermophysical properties of uranium dioxide*, Journal of Nuclear Materials, **279**(1): 1-18, 2000.

[81] C. Duriez et al., *Thermal conductivity of hypostoichiometric low Pu content (U,Pu)*$O_{2-x}$ *mixed oxide*, Journal of Nuclear Materials, **277**(2-3):143-158, 2000.

[82] P. R. Vasudeva Rao et al,*Oxygen potential and thermal conductivity of (U, Pu) mixed oxides*, Journal of Nuclear Materials, **348**(3):329-334, 2006.

[83] Masato Kato and Kenji Konashi, *Lattice parameters of (U, Pu, Am, Np)$O_{2-x}$*, Journal of Nuclear Materials, **385**(1):117-121, 2009.

[84] Kyoichi Morimoto et al, *Thermal conductivities of (U, Pu, Am)$O_2$ solid solutions*, Journal of Alloys and Compounds, **452**(1): 54-60, 2008.

[85] Y. Arai et al., *Dependence of the thermal conductivity of (U, Pu) N on porosity and plutonium content*, Journal of Nuclear Materials, **195**(1-2): 37-43, 1992.

[86] P. G. Lucuta, Hj. Matzke and J. Hastings, *A pragmatic approach to modelling thermal conductivity of irradiated $UO_2$ fuel: review and recommendations*, Journal of Nuclear Materials, **232**(2-3): 166-180, 1996.

[87] Yasuo Arai et al., *Thermal conductivity of neptunium mononitride from 740 to 1600 K*, Journal of Nuclear Materials, **211**(3): 248-250, 1994.

[88] V. Basini, J. P. Ottaviani, J. C. Richaud, M. Streitb and F. Ingold, *Experimental assessment of thermophysical properties of (Pu,Zr)N*, Journal of Nuclear Materials, **344**(1-3): 186-190, 2005.

[89] Y. S. Kim, G. L Hofman, S. L Hayes and Y. H Sohn, *Constituent redistribution in U-Pu-Zr fuel during irradiation*, Journal of Nuclear Materials, **327**(1):27-36, 2004.

[90] Steven B. Ross, Mohamed S. El-Genk and R.Bruce Matthews, *Uranium nitride fuel swelling correlation*, Journal of Nuclear Materials, **170**(2): 169-177, 1990.

[91] Kosuke Tanaka, Koji Maeda, Kozo Katsuyama, Masaki Inoue, Takashi Iwai and Yasuo Arai, *Fission gas release and swelling in uranium-plutonium mixed nitride fuels*, Journal of Nuclear Materials, **327**(2-3):77-87, 2004.

[92] International Atomic Energy Agency (IAEA), *Thermophysical properties of materials for nuclear engineering*, ISBN 978-92-0-106508-7, pp.14-18, 2008.

[93] M. Eriksson, J. Wallenius, M. Jolkkonen, J. Cahalan, *Inherent safety of fuels for accelerator-driven systems*, **151**(3): 314-333, 2005.

[94] W. J. Carmack, et al., *Metallic fuels for advanced reactors*, Journal of Nuclear Materials, **392**(2):139-150, 2009.

[95] Roger Thetford and Mike Mignanelli, *The chemistry and physics of modelling nitride fuels for transmutation*, Journal of Nuclear Materials, **320**(1-2): 44-53, 2003.

[96] J. J. Katz, G. T. Seaborg and L. R. Morss, The chemistry of the actinide elements, 2nd Edition, Vols. 1 and 2, Chapman and Hall, London, 1986.

[97] G. L. Hofman, L. C. Walters and T. H. Bauer, *Metallic fast reactor fuels*, Progress in Nuclear Energy, **31**(1-2):83-110, 1997.

[98] C. Sari, C. T. Walker, M. Kurata and T. Inoue, *Interaction of U-Pu-Zr alloys containing minor actinides and rare earths with stainless steel*, Journal of Nuclear Materials, **208**(3):201-210, 1994.

[99] R. L. Gibby et al., *Analytical expressions for enthalpy and heat capacity for uranium-plutonium oxide*, Journal of Nuclear Materials, **50**(2): 155-161, 1974.

[100] C. Thiriet, R. J. M. Konings, *Chemical thermodynamic representation of* $AmO_{2-x}$, Journal of Nuclear Materials, **320**(3): 292-298, 2003.

[101] T. Matsui and R. W. Ohse, *Thermodynamic properties of uranium nitride, plutonium nitride and uranium-plutonium mixed nitride*, High Temp-High Press, **19**, 1987) 1.

[102] F. L. Oetting, *The chemical thermodynamic properties of nuclear materials III. Plutonium mononitride*, The Journal of Chemical Thermodynamics, **10**(10): 941-948, 1978.

[103] Tsuyoshi Nishi et al., *Thermal diffusivity of Americium mononitride from 373 to 1473 K*, Journal of Nuclear Materials, **355**(1-3): 114-118, 2006.

[104] R. J. M. Konings, *The high-temperature heat capacity of americium*, Journal of Alloys and Compounds, **348**(1-2):38-42, 2003.

[105] R.F. Redmond and J. Lones, *Enthalpies and heat capacities of stainless steel (316), zirconium, and lithium at elevated temperatures*, ORNL-1342, Reactor Experiemntal Engineering Division, Oak Ridge National Laboratory, pp.8-9, 1952.

[106] Giacomino Bandini et al., *Decay Heat Removal and Transient Analysis in Accidental Conditions in the EFIT Reactor*, Science and Technology of Nuclear Installations, Volume 2008, Article ID 681847, 2008.

[107] US Department of Energy (DOE), *A Roadmap for Developing Accelerator Transmutation of Waste (ATW) Technology - A Report to Congress*, DOE/RW0519, 1999.

[108] Y. Ando, K. Nishihara, H. Takano, *Estimation of spent fuel compositions from light water reactors*, **37**:924-933, 2000.